The lunar Neon exosphere seen in LACE data

Rosemary M. Killen[a]*, David R. Williams[b], Jaekyun Park[c], Orenthal J. Tucker[a], Sang-Joon Kim[c]

[a]NASA Goddard Space Flight Center, Code 695, Greenbelt, MD 20771, USA

[b]NASA Goddard Space Flight Center, Code 690.1, Greenbelt, MD 20771, US

[c]School of Space Research, Kyung Hee University, Yongin 446-701, Republic of Korea

Submitted to Icarus on June 21, 2018

Revised March 28, 2019

1. Introduction

Apollo 17 carried a miniature mass spectrometer, called the Lunar Atmospheric Composition Experiment (LACE), to the Moon as part of the Apollo Lunar Surface Experiments Package (ALSEP) to study the composition and variations in the lunar atmosphere. The instrument was deployed in the Taurus-Littrow Valley (TL) with its entrance aperture oriented upward to measure the downward flux of gases at the lunar surface. The instrument was turned on December 27, 1971, 50 hours after sunset, and operated throughout the lunar night. The advent of sunrise brought a high background gas level, thus operations were discontinued during lunar daytime except for a brief check near noon. Operation was resumed near sunset and continued throughout the nights for the second through ninth lunations. Details of the experiment are in the Final Report, NASA-CR-150946 (Hoffman, 1975).

The data from the LACE experiment were downloaded and archived at the NASA Space Science Data Coordinated Archive (NSSDCA). Our Monte Carlo models assuming a solar wind source reproduce the trend observed in the second and third lunations but not the magnitude. The trend

seen in the fourth and fifth lunations is decreasing during the lunar night and cannot be reproduced unless the solar wind source is reduced or lost to the surface.

2. Data Calibration

LACE measured mass per unit charge, thus there is an ambiguity between a mass with a single charge and an atom or molecule having double that mass which is doubly ionized. The LACE data were available for mass/charge (M/Q) 1 to 100, but the usable data are in the range 16 - 45 AMU/Q. For a given mass number a measurement was made every 13.5 minutes. The raw data are in counts per 0.6 second. The first task was therefore to calibrate the data. There is no available calibration for the LACE mass spectrometer data, however, a similar instrument was constructed and flown on the Pioneer Venus mission. The relative sensitivity graph attached below was constructed for that instrument on Pioneer Venus by integrating isotopic ratio errors (Donahue and Hodges, 1992). The available curve was used by Hodges et al. (1974) for Ar. We inserted lines to measure the transmission coefficients for mass 16 to 45 (Figure 1). As the transmission coefficient increases, the ions/count decreases. In other words, the transmission is a function of the efficiency of the measurement. We calculated conversion scale for those ions that we wanted to include in this study. Given that the argon sensitivity was exactly 100 atoms/cc per data count (Hodges, personal

53 communication) we derived a conversion scale using the ratio of their transmission coefficients as
54 shown in Figure 1 for the Pioneer Venus calibration. The ratios of transmission coefficients for
55 masses 16 to 110 are shown in Figure 1, and the ratios read off the curve are listed in Table 1. For
56 example, m22_counts=(m22_trscoeff/m40transcoef)*100. Although this may not be a precise
57 value, it is the best we could estimate from the Pioneer Venus curve. We note that because our
58 analysis is not particularly sensitive to the exact numbers, but rather relative values, precise
59 calibrations will not alter our conclusions.
60
61 First, if one assumes that M/Q=22 is ^{22}Ne and is uncontaminated and M/Q=20 contains both ^{20}Ne
62 and HF, then the ^{20}Ne abundance is calculated given the known isotopic ratio of ^{22}Ne and ^{20}Ne
63 where ^{20}Ne is 90.48% of all Ne and ^{22}Ne is 9.25% of all neon (Grimberg et al., 2008). Given that
64 the transmission coefficient of ^{22}Ne is 2.1 and the transmission coefficient of ^{20}Ne is 2.5, we derive
65 that the sensitivity of ^{22}Ne is 50 atoms/count and the sensitivity of ^{20}Ne is 40 atoms/count.
66 Examination of the LACE raw data (Supplemental material) shows there was significant
67 background noise during the measurements of masses lower than ~ 35 amu. This noise ramped up
68 with decreasing mass, and it was attributed to electronic disturbances from unshielded high voltage
69 wires and collectors (Apollo 17 mission evaluation team). To this end, a mass 22 peak was
70 identified at each 0.6 second integration period within the shifted mass range (25 – 26 amu). Then

71 local minima about the peak were used to estimate the background contribution weighted more
72 towards lower masses. The background contribution was then subtracted from the mass peak to
73 calculate the ^{22}Ne density. The corrected background subtracted counts in bin 22 vary from about
74 2 - 10. Hoffmann et al. (1975) used a similar approach to subtract the background noise, however
75 they obtained counts more than an order of magnitude larger. The density of ^{20}Ne must be 9.78
76 times that for ^{22}Ne. We justify the assumption of contamination of the mass 20 bin by two lines of
77 reasoning. First, the Rosetta Orbiter Spectrometer for Ion and Neutral Analysis (ROSINA) mass
78 spectrometer onboard the Rosetta spacecraft continued to outgas for many years even in the cold
79 outer solar system. Although the most important contaminant during the first 200 days of the
80 mission was water, there is a strong peak at mass 19 corresponding to fluorine, reported to be an
81 internal source (Schlappi et al, 2010).

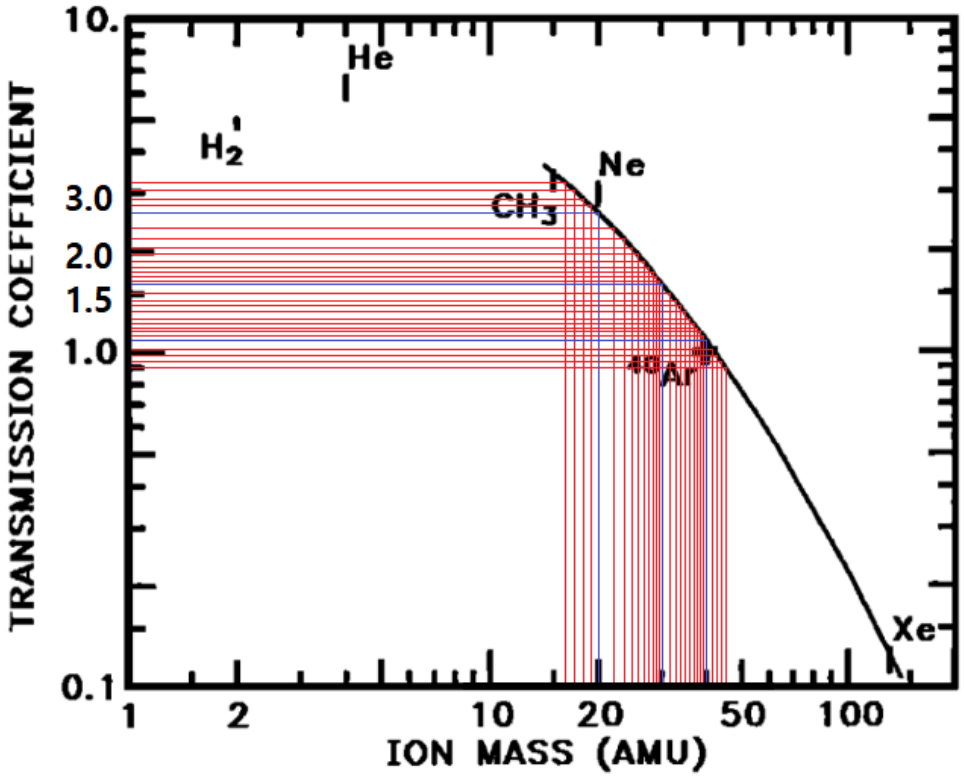

Figure 1. Transmission coefficients used for ion mass to charge, M/Q, 1 - 100 AMU based on Pioneer Venus neutral mass spectrometer.

Table 1. Transmission Coefficients for Mass numbers 16 - 45

Mass 16	3.1	Mass 26	1.8	Mass 36	1.2
Mass 17	3.0	Mass 27	1.7	Mass 37	1.1
Mass 18	2.9	Mass 28	1.7	Mass 38	1.1
Mass 19	2.7	Mass 29	1.6	Mass 39	1.1

Mass 20	2.5	Mass 30	1.6	Mass 40	1.05
Mass 21	2.2	Mass 31	1.5	Mass 41	1.0
Mass 22	2.1	Mass 32	1.4	Mass 42	1.0
Mass 23	2.0	Mass 33	1.4	Mass 43	0.9
Mass 24	2.0	Mass 34	1.3	Mass 44	0.9
Mass 25	1.9	Mass 35	1.2	Mass 45	0.9

88

89

90 **3. Nightside Ne densities**

91 Nightside densities were plotted from approximately dusk to dawn for four lunations, the second
92 through the fifth in the LACE data. The surface temperatures were read from the thermocouple
93 placed on the surface near the mass spectrometer. The data were measured every 0.6 second. We
94 determined dusk to be the time when the temperature plummeted and dawn where temperature
95 rose abruptly. The plots of neon density through the night for lunations 2 and 3 are shown in
96 Figure 2; those for lunations 4 and 5 are shown in Figure 3.

97

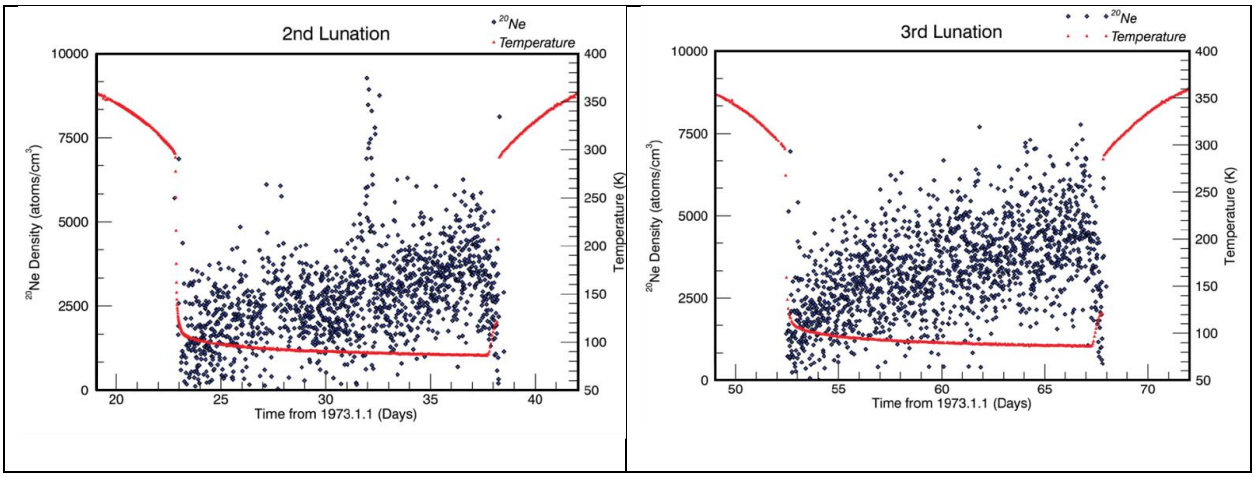

98

99 **Figure 2.** The ^{20}Ne densities measured on the second (left) and third (right) lunations are plotted

100 on the nightside from dusk to dawn (blue dots). The red lines are the temperature on the surface

101 measured by the thermocouple placed as part of the ALSEP package. We determined dusk by the

102 time the temperature dropped and dawn where the temperature suddenly rose.

103

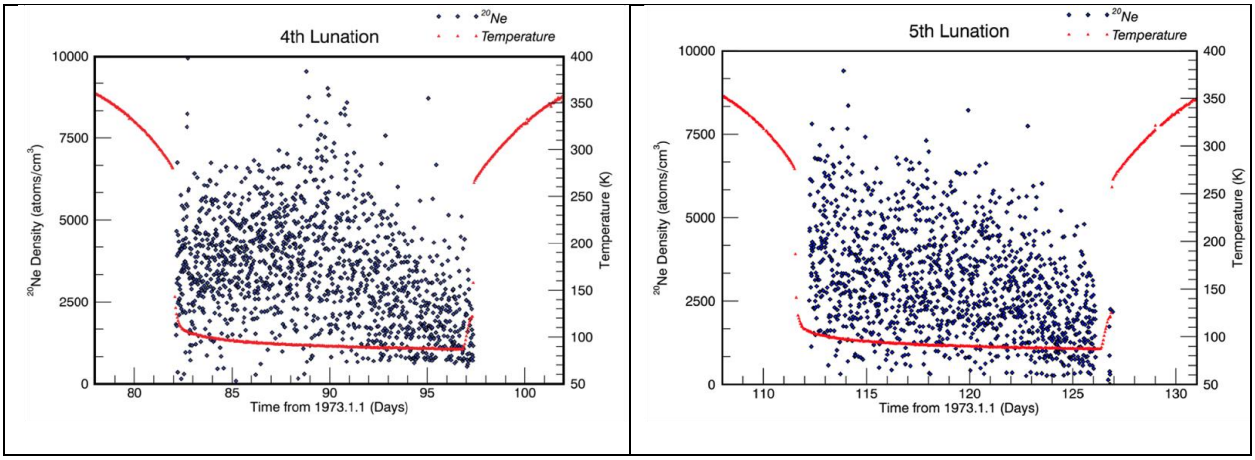

Figure 3. The ^{20}Ne densities measured on the fourth (left) and fifth (right) lunations are plotted on the nightside from dusk to dawn (blue dots). The neon densities for these lunations decreased during the night, in contrast to the variation on the second and third lunations.

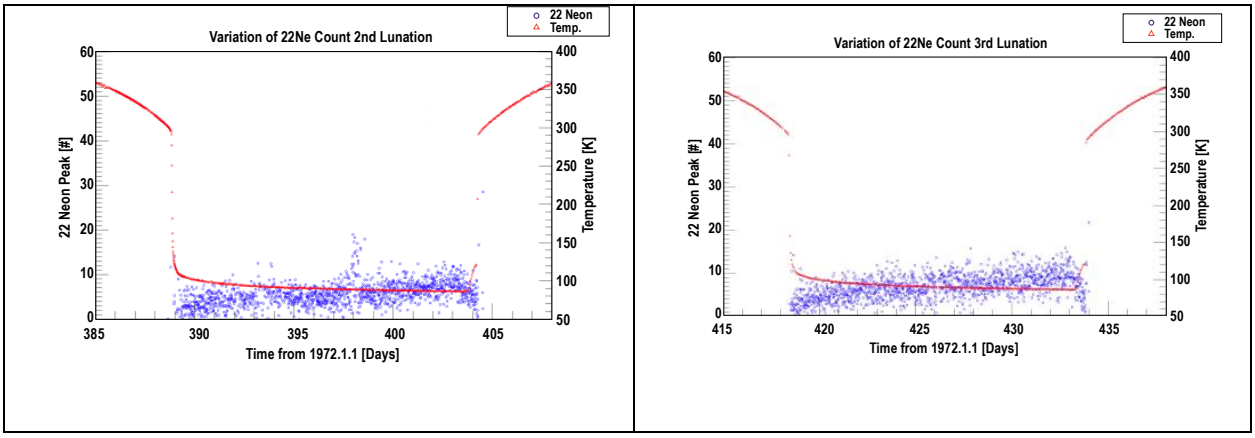

Figure 4. ^{22}Ne counts for second and third lunations after background subtraction, which were used to estimate the true ^{20}Ne density.

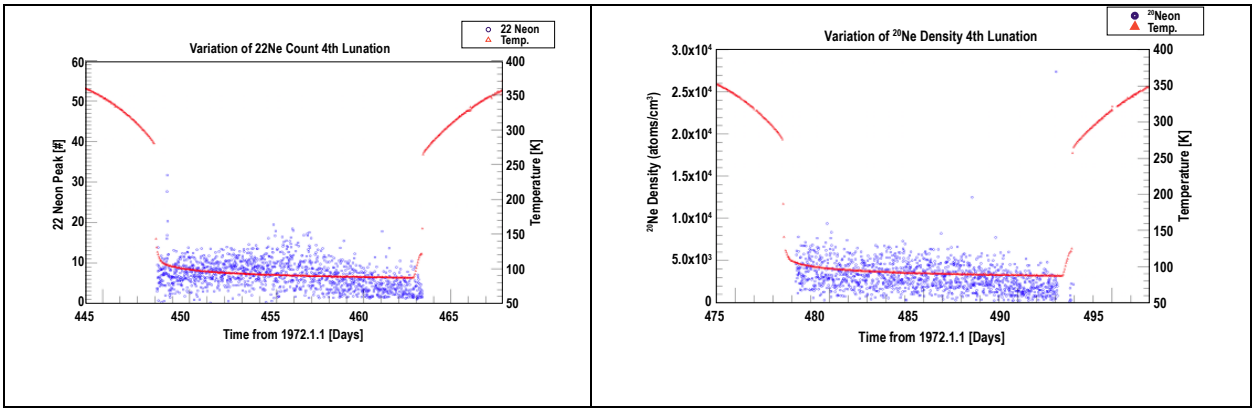

Figure 5. ^{22}Ne counts for the fourth lunation after background subtraction (left), which were used to estimate the true ^{20}Ne density (right).

The neon densities on the second and third lunations increase during the night from dusk to dawn. This is consistent with the results from Benna et al. (2015) and with theory of an exosphere in thermal equilibrium with the surface (Hodges, 1973). However, on the fourth and fifth lunations the neon density decreased from dusk to dawn. This is not consistent with previously published model results, but the measurement was also noted by Hodges et al. (1974).

Table 2. ^{20}Ne densities estimated for lunations 2 - 5

Lunation	Dates	^{20}Ne Density
2nd	Jan. 24 - Feb. 8, 1973	$(1.5 - 3.5) \times 10^3$ atoms/cm^3
3rd	Feb. 22 - Mar. 9, 1973	$(2.0 - 4.5) \times 10^3$ atoms/cm^3
4th	Mar. 24 - Apr. 8, 1973	$(2.0 - 4.0) \times 10^3$ atoms/cm^3
5th	Apr. 23 - May 7. 1973	$(2.0 - 4.0) \times 10^3$ atoms/cm^3

5. Implication of solar wind impact for Neon

Neon is carried to the Moon with the solar wind. For normal solar wind conditions near solar minimum, Ne/O=0.17, O/H=4.86x10^{-4} (Shearer et al., 2014). For normal slow wind speed (v_{sw}=400 km/s) and density (N_{sw}=5 cm^{-3}), the solar wind influx of ^{20}Ne is 8.2x10^{-5}(N_{sw} v_{sw}), or

127 $1.6x10^4$ cm^{-2} s^{-1}. The solar wind composition in a Coronal Mass Ejection (CME) driver gas is given
128 in Table 5 of von Steiger et al. (2000). The photoionization rate for Ne depends on the solar
129 ionizing flux and is therefore dependent on the solar cycle. It is listed as $1.1x10^{-7}$ s^{-1} in 1978 and
130 $5.x10^{-7}$ s^{-1} in 2002 (Bochsler, 2014). The solar cycle was approximately the same in 1972 as in
131 1978 except that in 1972 the solar cycle was in its declining phase and on 1978 the solar cycle was
132 increasing. The Ne photoionization lifetime was thus about $9x10^6$ seconds, 100 days, or 3.4
133 months, for our observations.
134
135 Benna et al. (2015) measured the Ne abundance in the lunar exosphere with Lunar Atmosphere
136 Dust and Environment Explorer (LADEE) Neutral Mass Spectrometer (NMS) during the Coronal
137 Mass Ejection (CME) period of 7-27 Feb. 2014. The surface number density for Ne given by
138 Benna et al. (2015) is n_0= $2x10^4$ cm^{-3} about an order of magnitude more than our average value (2
139 - 4 $x10^3$) and that of Cook et al. (2013) ($4.4x10^3$ cm^{-3}). Hodges et al., (1974) reported a nightside
140 density of ^{20}Ne of 10^5 cm^{-3} and a theoretical nightside density of $1.1x10^5$ cm^{-3} (Hodges, 1973)
141 almost two orders of magnitude higher than our measured nominal value, (1.5 - 4.5)$x10^3$ atoms
142 cm^{-3}. The Benna et al. (2015) value was reported to be observed during a CME. Because
143 photoionization does not occur on the nightside, the average photoionization lifetime over the
144 entire lunation should be multiplied by 2 in the analytical aproximation, so that the abundance in

the exosphere depends on the solar wind flux over the preceding 6 months rather than 3 months. Because only lunar night time LACE observations were used, none of those observations were taken when the Moon was in the Earth's geomagnetic tail where the solar wind would not impact the lunar surface.

6. Model

We adapted the Monte Carlo model used in Tucker et al. (2015, 2019) in order to model the global concentration of neon in the Moon's exosphere. It is assumed that neon implanted by the solar wind is balanced by neon degassed from the surface. The computational domain is centered on the moon and discretized in spherical coordinates with a radial increment of 12 km and azimuthal and zenith increments of ~5 degrees. The moon is chosen as an inertial frame, and illumination of the surface is tracked assuming an average lunar day equivalent to 29.5 Earth days. For the model, the local surface temperature was estimated using $T(Z) = 250\ K*\cos^{1/4}(Z) + 100\ K$, where Z is the solar zenith angle (Butler, 1997; Crider and Vondrak, 2002). The neon source flux from the soil on the illuminated hemisphere is assumed to be equivalent to the incident SW flux ^{20}Ne is $8.2x10^{-5}(N_{sw}\ v_{sw})\cos(Z)$. Representative molecules are emitted isotropically from each surface element using the Maxwell Boltzmann Flux speed distribution at the local surface temperature with a cosine angular distribution to direct the velocities (Brinkmann, 1970). If a computational particle

was traveling faster than the escape speed at radial distances above 1800 km it was removed from the simulation. However, thermal escape is negligible for neon, so the dominant loss mechanism was photoionization. When particles hit the surface, they are assumed to be accommodated to the surface temperature and diffusely scattered.

Three simulations were carried out in the analyses of the LACE measurements. To this end, we tracked the exosphere density at 20 degrees latitude as a function of lunation. The model data plotted in Figure 6 were obtained by averaging the neon density within ½ a scale height of the surface at the TL latitude over time intervals of 1.5 hours. Note we obtained a similar result using averages collected over a shorter 30-minute time intervals, however to reduce the scatter due to model statistics we show the results obtained using the larger interval. Simulation (1) was carried out using the normal (averaged) solar wind flux of $8.2 \times 10^{-5} (N_{sw}\ v_{sw}) \cos(Z)$ and the actual photoionization lifetime of 3.4 months, Figure 6a. However, the predicted ^{20}Ne densities were over an order of magnitude larger than the LACE measurements. We found an exospheric lifetime of ~4.5 days for ^{20}Ne was required to obtain densities on the same magnitude as the LACE measurements shown in Simulation (2), Figure 6b. Lastly, in Simulation (3) we consider temporal variations using OMNI data of the variable solar wind during lunations 2 – 5 with the lifetime of ~4.5 days. The results obtained in Simulation (3) are shown in the supplementary information.

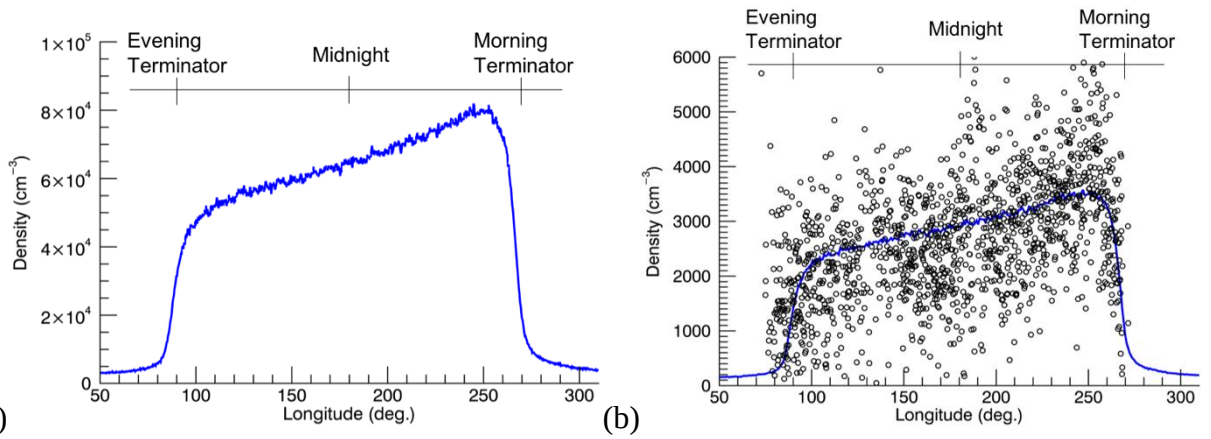

Figure 6: Simulation (1) 6a and (2) 6b of neon density at TL using the averaged SW flux $N_{SW}v_{SW}(Ne) = 1.65 \times 10^4$ cm^{-2}s^{-1} and the photoionization lifetime of 100 days (a) and 4.5 days (b). We obtained a peak density of ~7.9 x10^4 cm^{-3} and ~3800 cm^{-3} that occurred ~40 hours before the dawn terminator (~250^0 longitude) for Simulation (1) and (2), respectively. Simulation (1) modeled result is consistent with Hodges et al. (1974) estimate of 1.1x10^5 cm^{-3}, which used a neon ion flux that was a factor of 1.5 larger. However, Simulation (2) using the artificial lifetime obtains results more consistent with LACE measurements during lunations 2 and 3, and the upper limit of densities observed near dawn by LAMP (Cook et al. 2013).

7. Conclusions

The measured densities were consistent with the ^{20}Ne column densities reported by Cook et al. (2013) for normal conditions. This is an order of magnitude less than those reported by Benna et al. (2015) for CME conditions. Our Monte Carlo code employing the assumption of a 100 day photoionization lifetime and no surface adsorption results in densities a factor of 2 - 4 larger than the Benna et al. (2015) measurements. For CME conditions, the solar wind would have an enhanced abundance of heavy ions such that Ne/O =0.32 and O/H=$3x10^{-4}$. If v_{sw}=800 km/s and N_{sw}=10 cm^{-3} as expected for the CME, then the solar wind Ne flux to the lunar surface would be Ne = $7.7x10^4$ cm^{-2} s^{-1}. However, using the actual photoionization lifetime of 100 days, and a nominal SW flux $N_{SW}v_{SW}$(Ne) = 1.65 $x10^4$ cm^{-2} s^{-1} the Ne density just before dawn would have been $8x10^4$ cm^{-3} consistent with the theoretical result from Hodges (1973) and twice that of the night time peak reported by Benna et al. (2015), which was attributed to a CME passage.

Using the non-uniform surface temperature T(Z)= 250*cos(Z) + 100K (e.g., Crider and Vondrak, 2002), where Z is the solar zenith angle, and applying the photoionization loss only on the dayside, the Monte Carlo model densities are a factor of ~20 larger at midnight compared to the LACE measurement. The OMNI data indicated the solar wind flux varied by a factor of ~10 on timescales

of hours to days during the LACE experiment. When using the OMNI data with an artificial lifetime of ~4.5 days, the resulting ^{20}Ne densities varied by less than 50% from that obtained using normal average solar wind conditions.

We could not reproduce the trend of the densities from dusk to dawn as measured during the 4th and 5th lunations. During those lunations the ^{20}Ne density continued to decrease during the night, in contrast to lunations 2 and 3 where the densities increased during the night, consistent with cooling throughout the night. Apparently, explaining the ^{20}Ne distribution is not as simple as assuming dynamic equilibrium with the solar wind and an exosphere accommodated to the local surface temperature. Furthermore, extracting the accurate abundance of Ne from in situ mass spectrometer data on the Moon remains an important topic of investigation. Neon is highly non-reactive so understanding its sources and sinks to the exosphere can directly inform us about the retention of atoms in the lunar regolith by physical defects and the energetics of space weather events.

An enhanced Ne measurement occurred during the night of 5th lunation when Taurus Littrow (TL) was located approximately 24 - 28 hours from the morning terminator. Therefore, in the simulation approximately 38 hours before TL rotated to dawn terminator the SW enhancement flux was elevated and the response of the exosphere was simulated. We initially thought that the increase

228 in M/Q 22 at the end of the fifth lunation before sunrise might have been due to outgassing of a
229 contaminant, possibly CO_2^{++} in the instrument near dawn or atoms hopping from the dayside to
230 the nightside. However, if CO_2^{++} (M/Q=22) is the result of ionization of CO_2^{+} (M/Q=44) then the
231 rise in 22 should have been 5% of the rise in M/Q=44 due to the known fractionation. Instead the
232 M22/M44 rise ratio was approximately 8.5.
233
234 We also see an increase in oxygen and hydroxyl at the same time as the increase in M/Q 22. The
235 increased counts at dawn at mass 20 could be MgO^{++}, Ar^{++}or Ca^{++} as well as ^{20}Ne. However, the
236 ratios of the measured species, which were measured as mass per charge, are strange and not
237 consistent with fractionation due to expected isotopic ratios. If the counts in bin 20 are not
238 contaminated, we can estimate the ^{20}Ne density by multiplying counts by 40, giving a ^{20}Ne density
239 of about $1.4x10^4$, fairly consistent with the sunrise ratio published by Benna et al. (2015) from
240 LADEE data. In addition to the measured ratios of M/Q 22 and 44, we cannot model the decrease
241 in M/Q 20 during the nightside for lunations 4 and 5. Therefore, we have shown that explaining
242 the Ne distribution is not as simple as assuming dynamic equilibrium with the solar wind and an
243 exosphere accommodated to the local surface temperature. This was also noted by Hodges et al.
244 (1974), who conclude that the failure of the Apollo 17 data to rise late in the night may indicate a
245 slight amount of adsorption. However, this does not explain the difference between lunations 2

and 3 and the lunations 4 and 5, respectively. We have shown that the enhanced solar wind flux cannot reproduce the observed rapid enhancement in Ne densities at dawn, and this is probably an artifact due to outgassing in the instrument.

Acknowledgements

RMK was supported by the DREAM2 Team of the NASA SSERVI Virtual Institute and by a grant from the NASA Solar System Observations program. OJT was supported by a NASA Postdoctoral Fellowship. SJK and JKP acknowledge support from the Space Core Technology program through NRF funded by the Ministry of Education, Science and Technology, Republic of Korea. We acknowledge use of NASA/GSFC's Space Physics Data Facility's OMNIWeb and OMNI data. We used data from the IMP-6 spacecraft in Earth orbit during the years 1971-1974. The LACE data are being archived in the NASA Planetary Data System Geophysics Node.

References

262 Benna, M., et al., 2015. Variability of helium, neon, and argon in the lunar exosphere as
263 observed by the LADEE NMS instrument. *Geophys. Res. Lett*. 42 #10, 3723-3729, 2015.
264 10.1002/2015GL064120.
265 Bochsler, P. et al., (2014). Solar photoionization rates for interstellar neutrals in the inner
266 heliosphere: H, He, O, and Ne. *Astrophys. Journ. Suppl.* 210 (12) 10 pp. doi:10.1088/0067-
267 0049/210/1/12
268 Brinkmann, R.T., 1970. Departures from Jeans escape rate for H and He in the Earth's
269 atmosphere. *Planet. Space Sci*. 18, 449–478.
270 Butler, B. J., (1997). The migration of volatiles on the surfaces of Mercury and the Moon. *J.*
271 *Geophys. Res.* 102, E8, 283 – 291.
272 Cook, J. C., et al., 2013. New upper limits on numerous atmospheric species in the native lunar
273 atmosphere. *Icarus* 225, 681-687, 2013.10.1016/j.icarus.2013.04.010
274 Crider, D.H. and Vondrak, R.R., 2002. Hydrogen migration to the lunar poles by solar wind
275 bombardment of the Moon. *Adv. Space Res*. 30 (8), 1869–1874.
276 Donahue, T. and R. R. Hodges., 1992. Past and present water budget of Venus. *Journ.*
277 *Geophys.Res*.97 E4, 6083-6091, 1992 doi: 10.1029/92JE00343.
278 Grimberg, A, H. Baur, F. Buhler, P. Bochsler, and R. Wieler. 2008. Solar wind helium, neon, and
279 argon isotopic and elemental composition: Data from the metallic glass flown on NASA's

Genesis mission. *Geochim. Cosmochim. Acta* 72, 626-645, 2008. Doi: 10.1016/j.gca.2007.10.017

Hodges, R. R. Helium and hydrogen in the lunar atmosphere. *J. Geophys. Res.* 78, 8055, 1973.

Hodges, R. R., J. H. Hoffman, and F. S. Johnson. 1974. The Lunar Atmosphere. *Icarus* 21, 415 - 426.

Hoffman, J. H., 1975. *Lunar Atmospheric Composition Experiment Final Report.* NAS 9-12074, June 1, 1971- September 30, 1975.

King, J. H., N. Papatashvilli., 2018. Plasma Data from cohoweb. *CDAWeb*, Adnet Systems, NASA Goddard Space Flight Center, Greenbelt MD. Generated Feb. 15, 2018.

SchlaPpi, B., K. Altwegg, H. Balsiger et al., 2010. Influence of spacecraft outgassing on the exploration of tenuous atmospheres with in situ mass spectrometry. *Journ. Geophys. Res.: Space Physics*, 115 A12, doi: 10.1029/2010JA015734.

Smith, E. J., A. Barnes., 2018. *CDAWeb*, NASA JPL/AMES.

Shearer, P., et al., 2014. The solar wind neon abundance observed with ACE/SWICS and Ulysses/SWICS. *Astrophysical Journal*, *789*(1), [60]. DOI: 10.1088/0004-637X/789/1/60

Tucker, O. J., Johnson, R. E., 2009. Thermally driven atmospheric escape: Monte Carlo simulations for Titan's atmosphere. *Planet. Space Sci*. 57, 1889–1894.

Tucker, O. J., R. E. Johnson, and L. A. Young. 2015. Gas Transfer in the Pluto-Charon System: A Charon Atmosphere. *Icarus* 246, 291-297.

Tucker, O. J., Farrell, W. M., Killen, R. M., & Hurley, D. M. (2019). Solar wind implantation into the lunar regolith: Monte Carlo simulations of H retention in a surface with defects and the H2 exosphere. *Journal of Geophysical Research: Planets*, 124, 278–293. https://doi.org/10.1029/2018JE005805

von Steiger, R., N. A. Schwadron, L. A. Fisk, J. Geiss, S. Hefti, B. Wilken, R. F. Wimmer-Schweingruber, and T. H. Zurbuchen. 2000. Composition of the quasi-stationary solar wind flows from Ulysses/Solar Wind Ion Composition Spectrometer, *J. Geophys. Res.*, 105(A12), 27,217–27,238, doi:10.1029/1999JA000358.

Supplemental Information

S.1 Raw Data

When we processed the data, we had to be careful because the mass peaks were not consistently at the same mass. We therefore tracked the peak as a function of time. Some mass range data are shown in Table S1 for some masses. We looked at all lunations and tried to choose the general range that includes all peaks regardless of drifting.

Table S1. General mass range of data attributed to actual mass.

Mass (AMU)	General range (AMU)
20	23.94586 - 22.56437
22	26.22125 - 25.02938
24	27.033888 - 28.09032
25	27.900704 - 28.957136

26	28.740432 - 30.067744
27	29.823952 - 31.693024
28	31.124176 - 32.722368
40	42.365696 - 43.557568
43	44.424384 - 45.2912
44	44.911968 - 45.9684

There is a lot of noise in the data. Usually the background noise level gradually increases from near-mass 30 AMU/Q to the end of the data, like the plot below. Figure S1 shows the raw spectrum for 12 – 48 AMU in counts vs. line number. The x-axis is nearly linear in mass/charge.

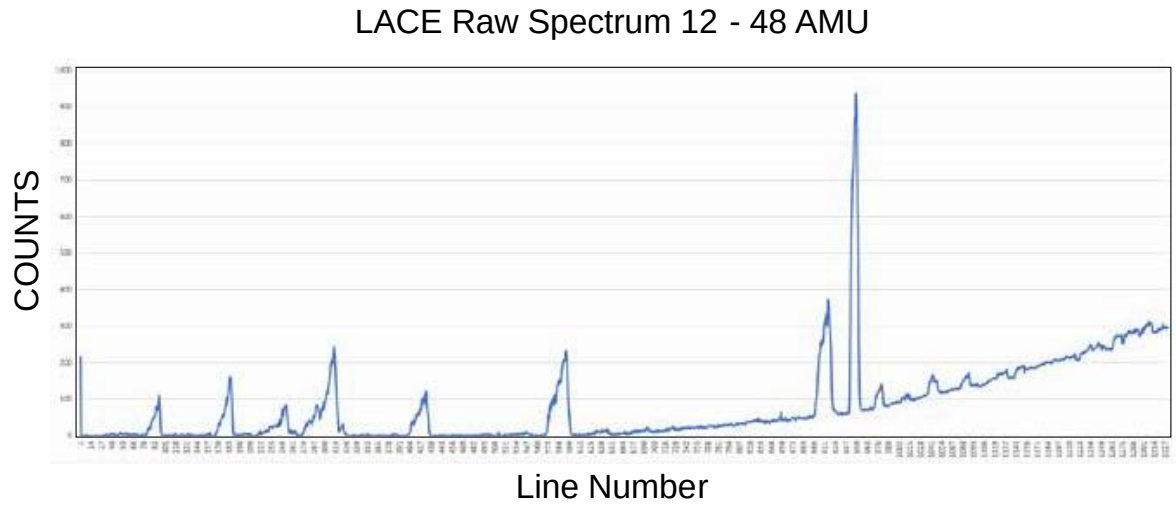

Figure S1. Sample raw spectrum 12-48 AMU.

S2. Calculating ^{20}Ne number density

We tried to find transmission coefficients of masses 22, 40 and 44 before calculating the number density of ^{20}Ne in the lunar atmosphere. We measured approximate values as follows:

$$m22\_trscoeff = 2.1 \;,\; m40\_trscoeff = 1.05 \;,\; m44\_trscoeff = 0.9 \quad \text{Eqn. S1}$$

where mxx_trscoeff is the counts per atom relative to 1.

Then, we calculated conversion scale for mass 22 and mass 44. Given that "*The argon sensitivity was exactly 100 atoms/cc per data count* " (Hodges, personal communication), we derived the conversion scales for mass 22 and mass 44 using the mass 40 transmission coefficient.

$$m22\_constant = 100.0/(m22\_trscoeff/m40\_trscoeff) \quad \text{Eqn. S2}$$

To multiply this conversion scale to ^{22}Ne counts that contribution of $CO_2{}^{++}$ had eliminated, we got the ^{22}Ne number density.

Eqn. S3

ne22 =

Because ^{20}Ne and ^{22}Ne have constant ratio in nature, we were finally able to derive the number density of ^{20}Ne.

Table S2. Main Isotopes of Ne

Isotope	Abundance (%)
^{20} Ne	90.48
^{21}Ne	0.27
^{22}Ne	9.25

ne20_ratio = 90.48 & ne22_ratio = 9.2

ne20 = ne22*ratio **Eqn. S5**

Now we have the number density of ^{20}Ne. The next step is data fitting of ^{20}Ne at the night time. Because of the anomaly of background noise, we used only 2nd, 3rd, first half of 4th, and very first part of 5th lunation to fit the slope of the density vs. time.

We tried to fit using Matlab routines LINFIT and LADFIT(Robust) for each lunation. Thus, we extracted the data of 2nd, 3rd, 4th, and 5th lunation and made each array. Then we eliminated erroneous values identified in the data sets with '-999 (N/A)' and other 'minus' values to do more precise fitting.

Finally, these are fittings of ^{20}Ne density in the night. The temperature (red curves) is read from the thermocouple placed on the surface of the Moon as part of the ALSEP package. Dusk is on the lefthand side of the plot and is determined by the sudden decline in temperature. Likewise

dawn, on the righthand side, is determined by the sudden temperature rise. The data were given in time since the instruments were turned on.

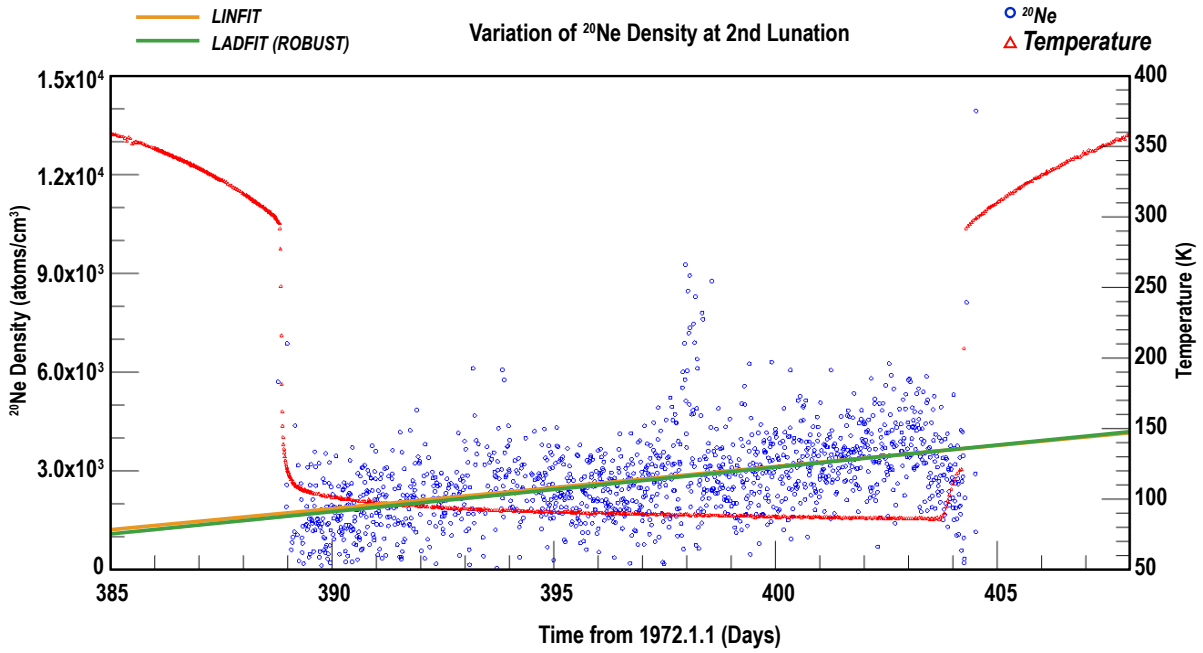

Figure S2. Variation of ^{20}Ne Density at 2nd lunation.

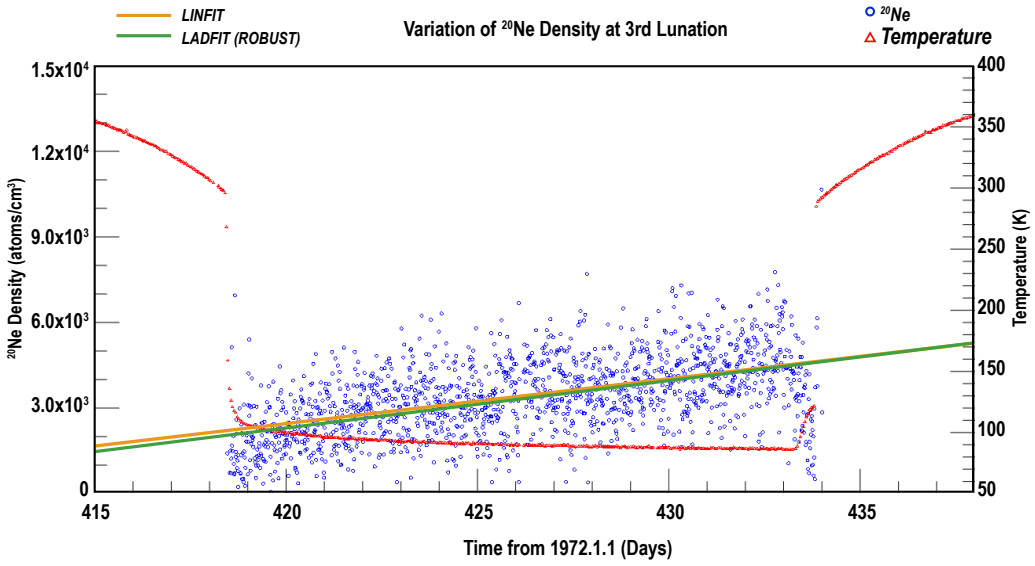

Figure S3. Variation of 20 Ne Density at 3rd lunation.

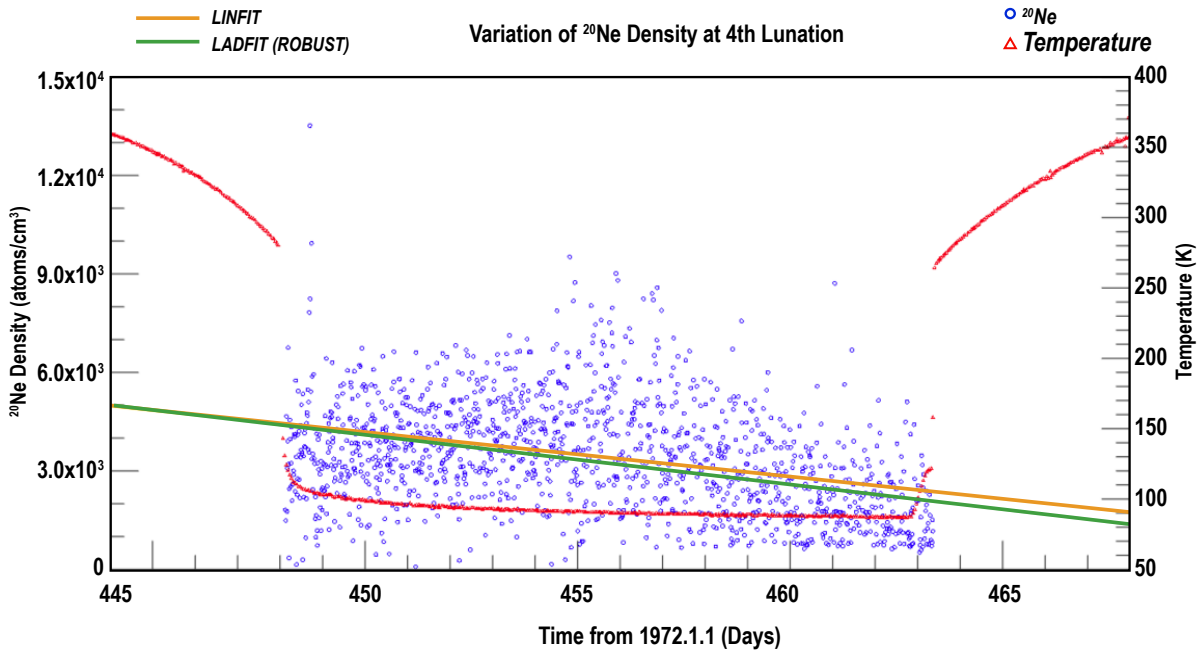

Figure S4. Variation of 20Ne at 4th lunation.

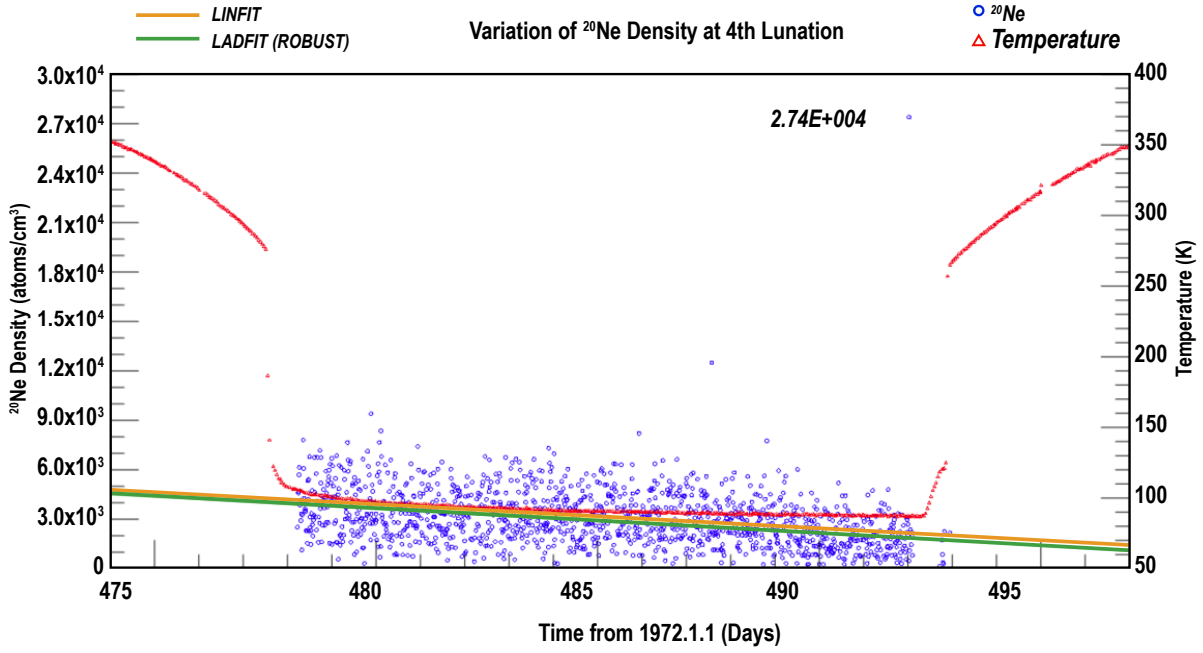

Figure S5. Variation of ^{20}Ne Density at 4th lunation showing sudden increase before dawn.

S.3 Sudden Increase in 5th lunation ; Implication of solar wind impact

When we looked closely at the variation of Mass 22 peak, we found something intriguing. There was sudden increase of peak in the later part of 5th lunation. Second half of 5th lunation was

mostly no peak but noise, however, the mass 22 peak suddenly appeared at the time of May 7th, 1973. We selected the 11 time-row around the increase point we found - May 7th, 00:38., and made a plot of it. This is the plot of all mass in Mid-Range. We were not sure whether this peak was a real ^{22}Ne peak or an increase due to warming near dawn.

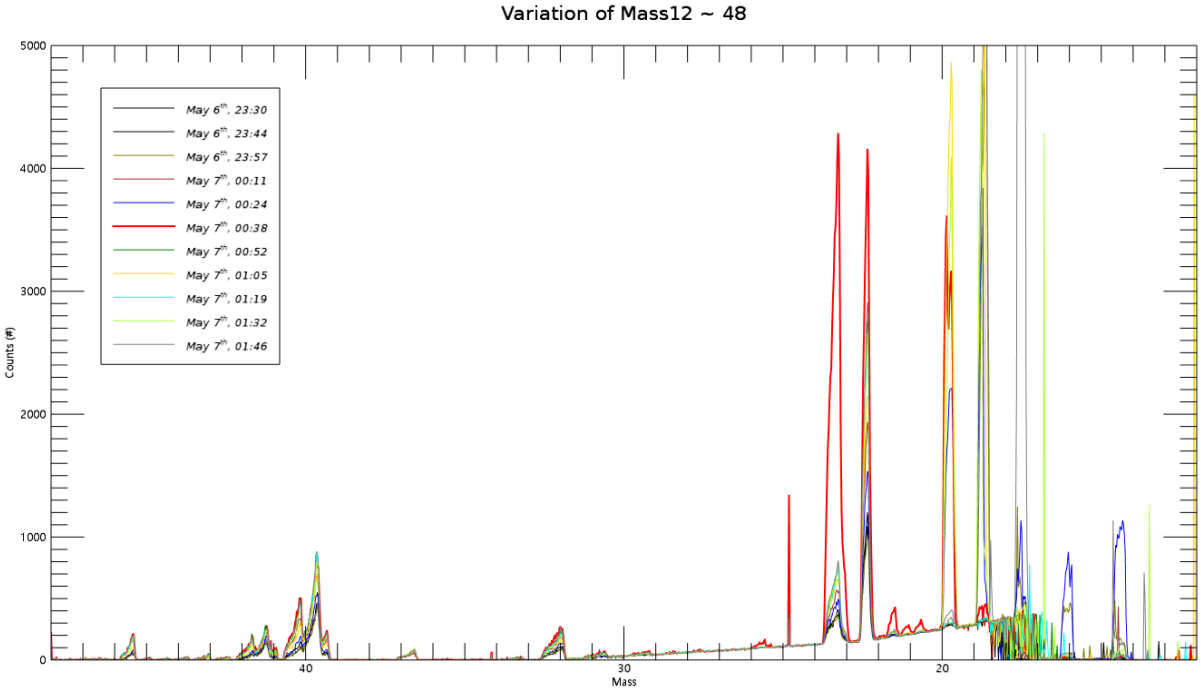

Figure S6. Variation of Mass 12 - 48 May 6 - May 7.

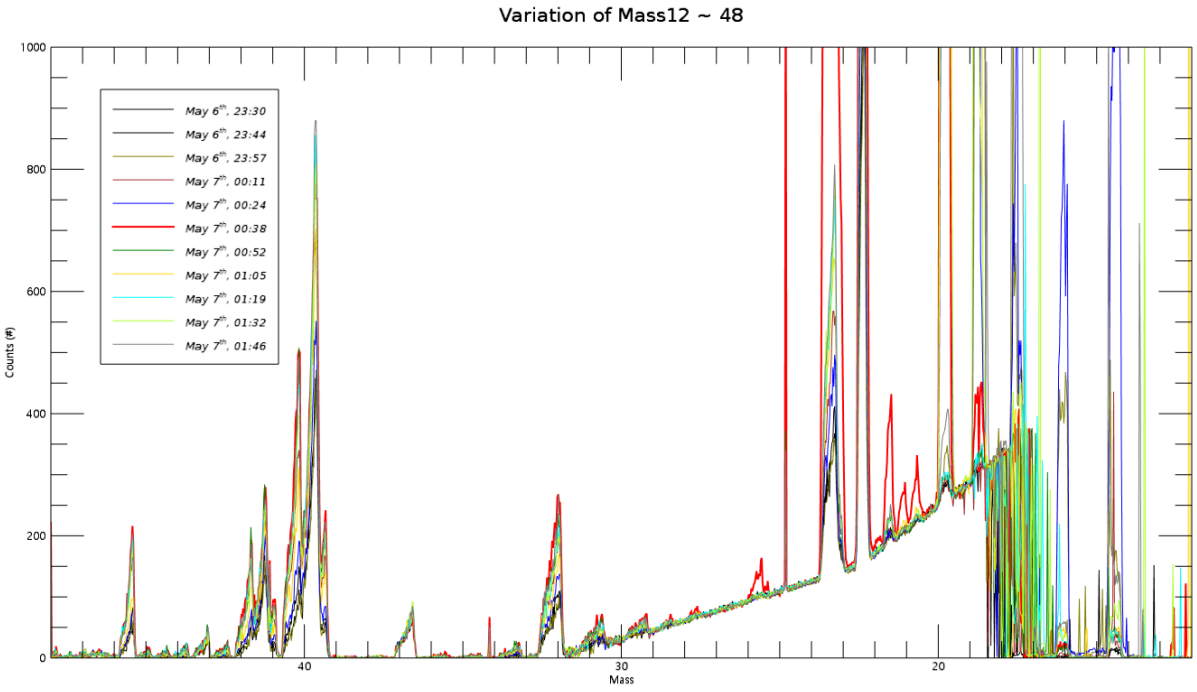

Figure S7. This is more magnified version of Figure S6.

• Mass 16

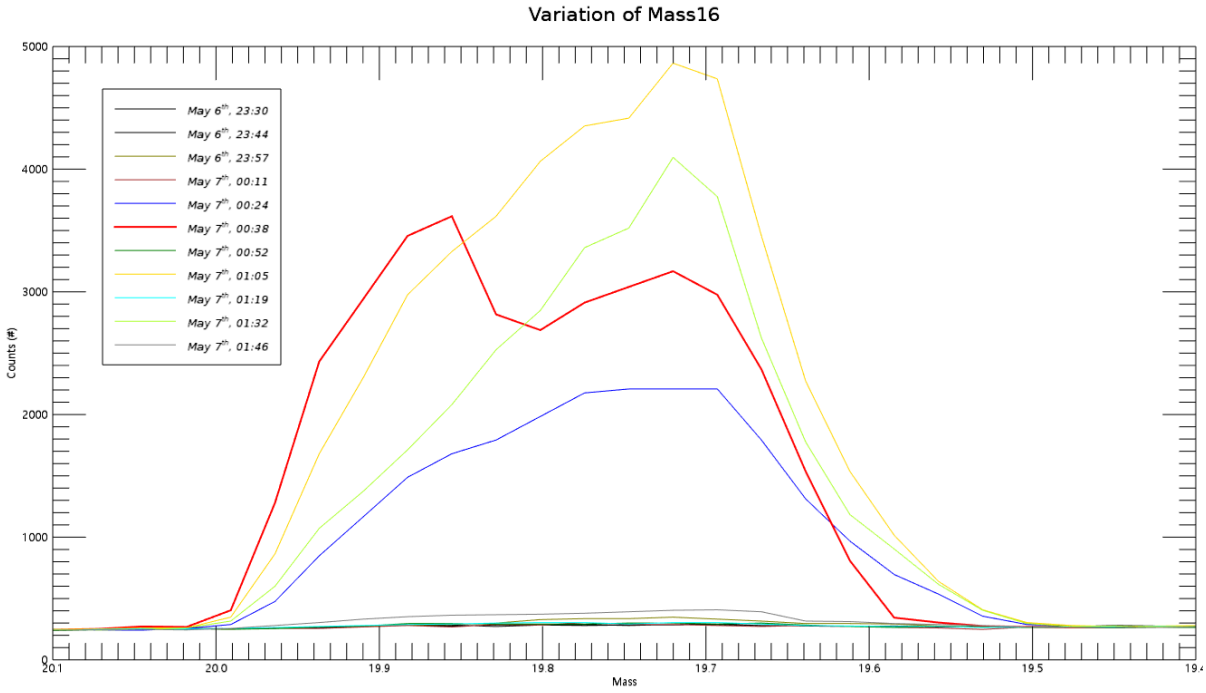

Figure S8. Variation in Mass 16 May 6 - May 7.

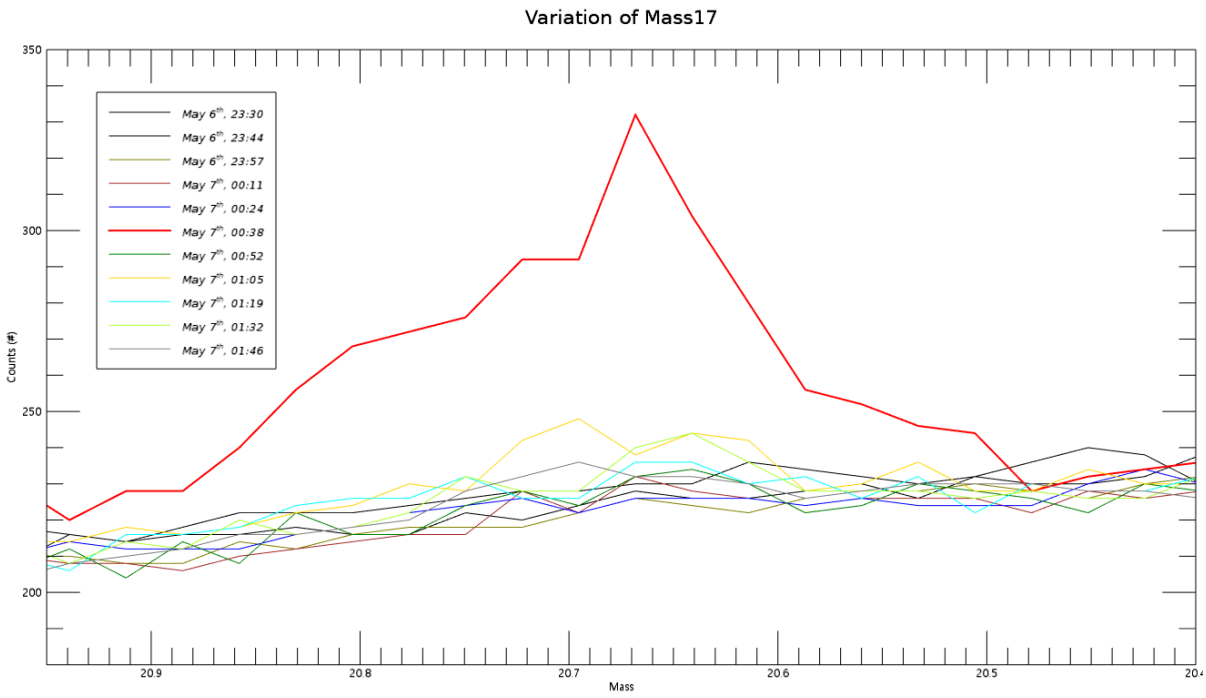

Figure S9. Variation of Mass 17 May 6 - May 7.

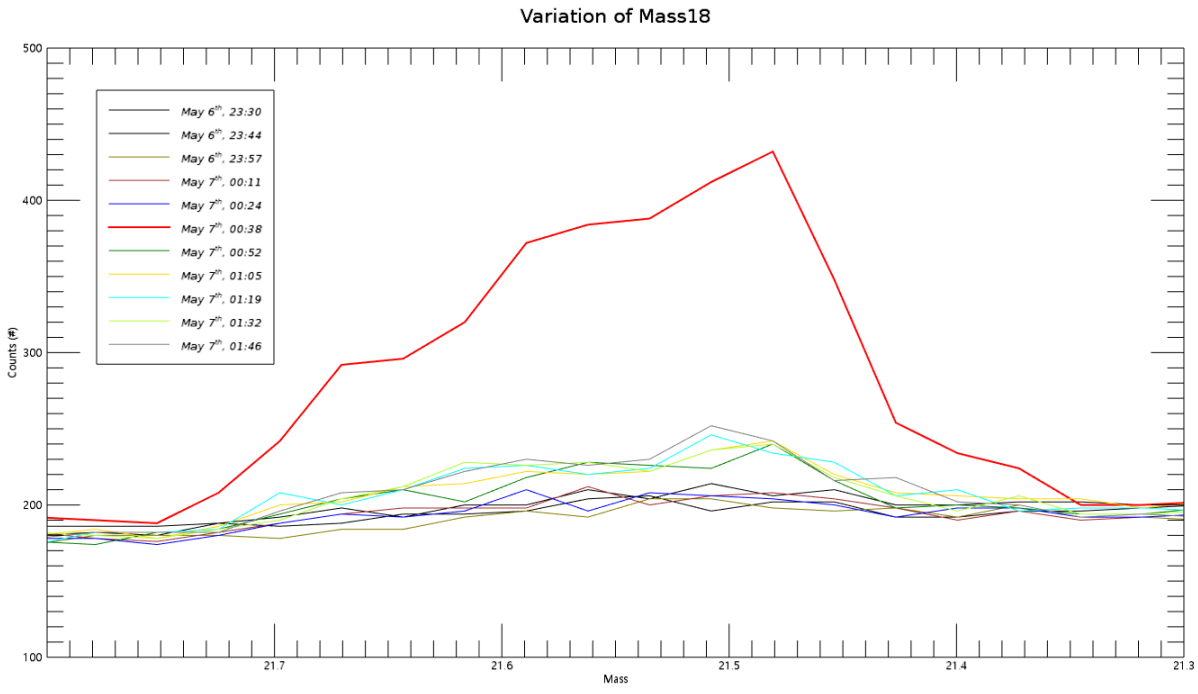

Figure S10. Variation of Mass 18 May 6 - May 7.

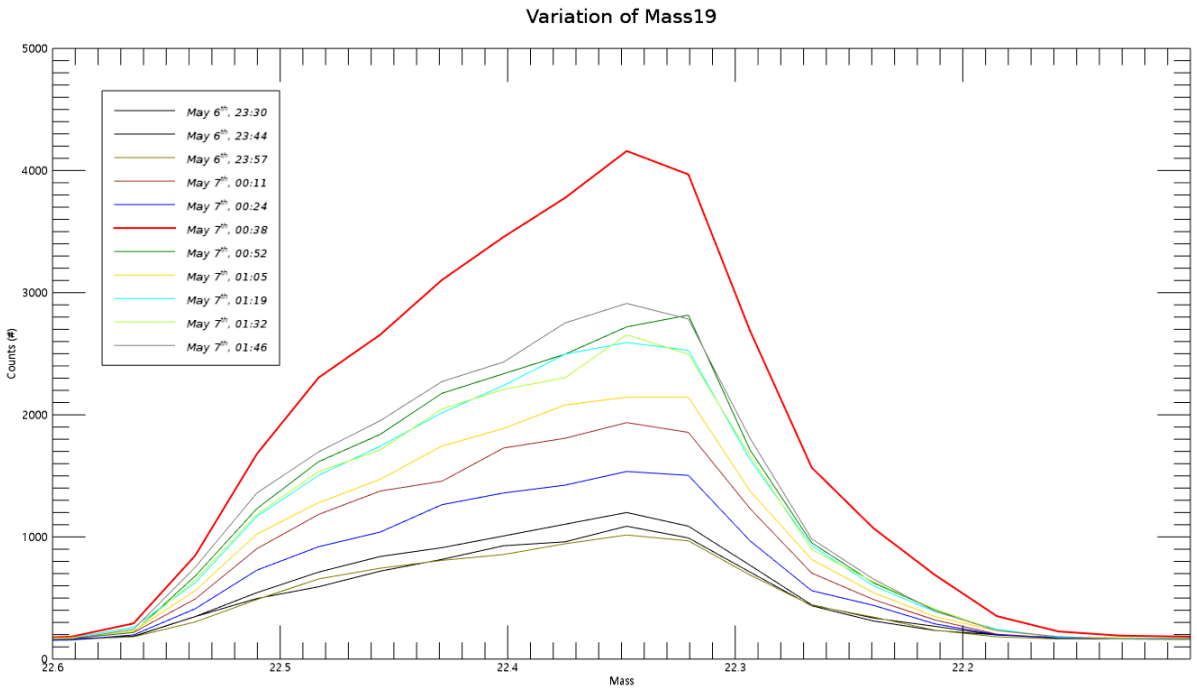

409

410 Figure S11. Variation of Mass 19 May 6 - May 7.

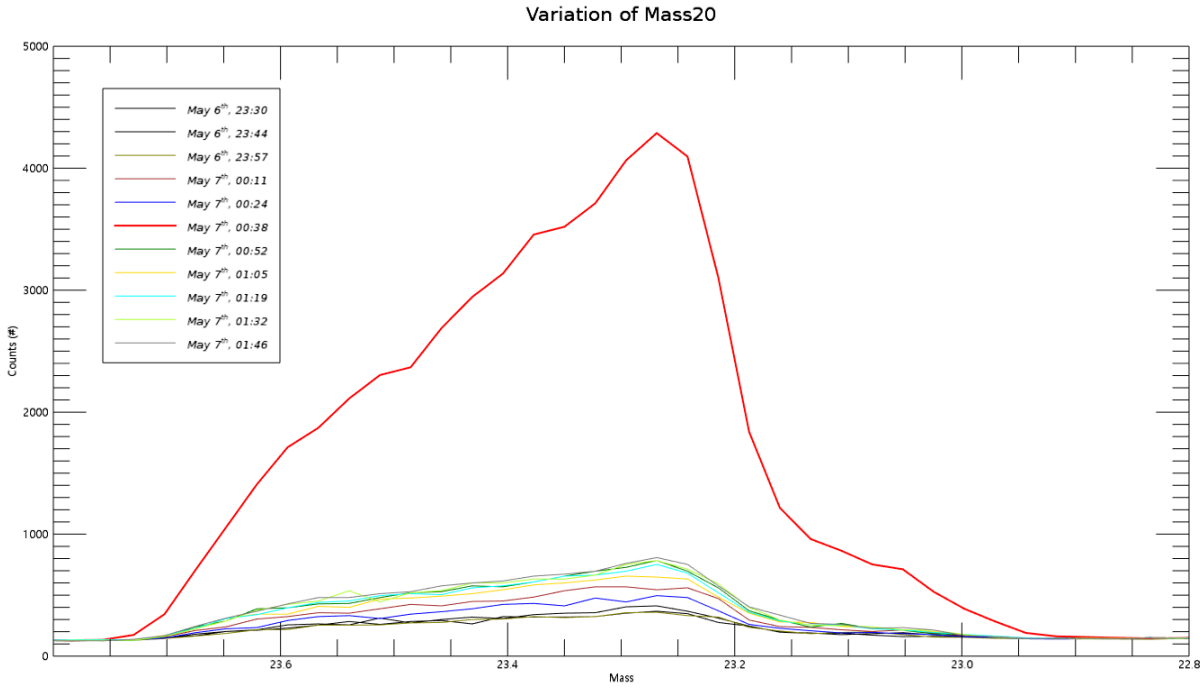

411

412 Figure S12.Variation of Mass 20 May 6 - May 7.

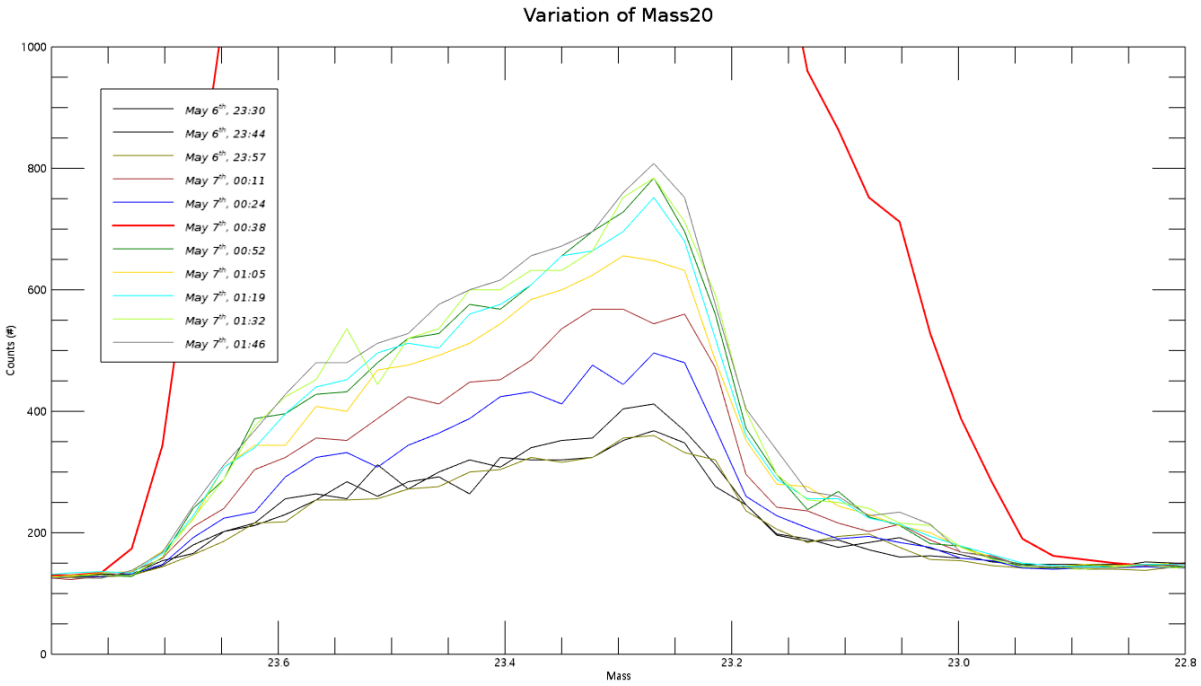

Figure S13.Variation of Mass 20 (magnified) May 6 - May 7.

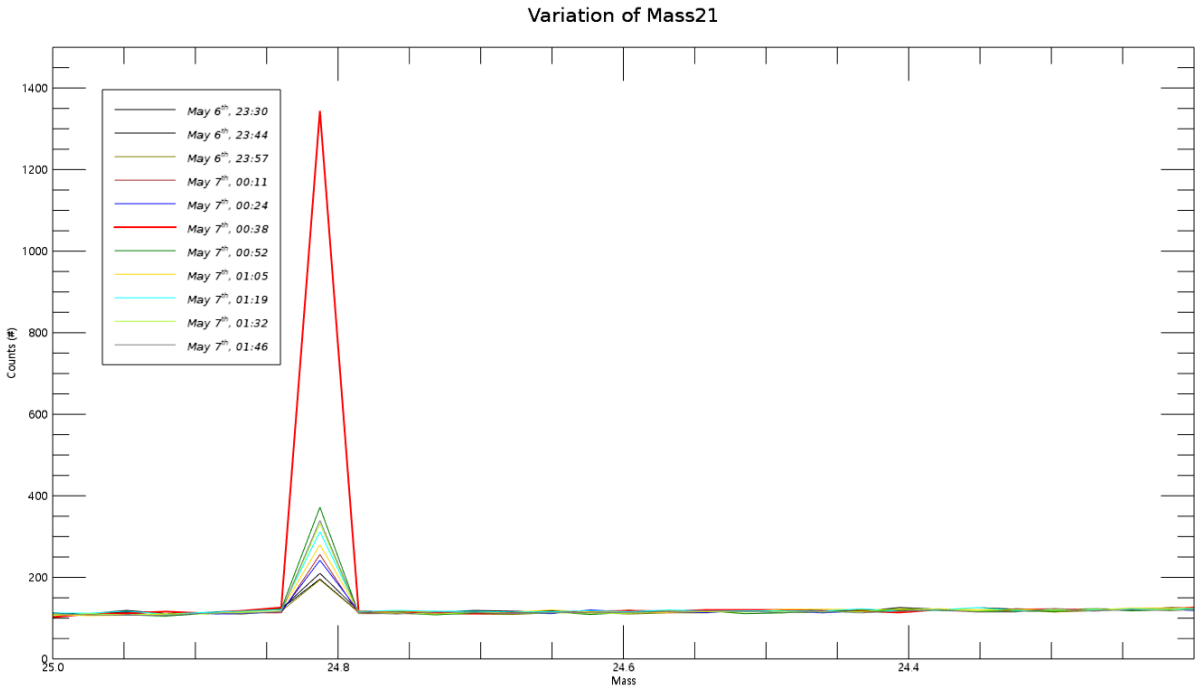

Figure S14.Variation of Mass 21 (noise) May 6 - May 7.

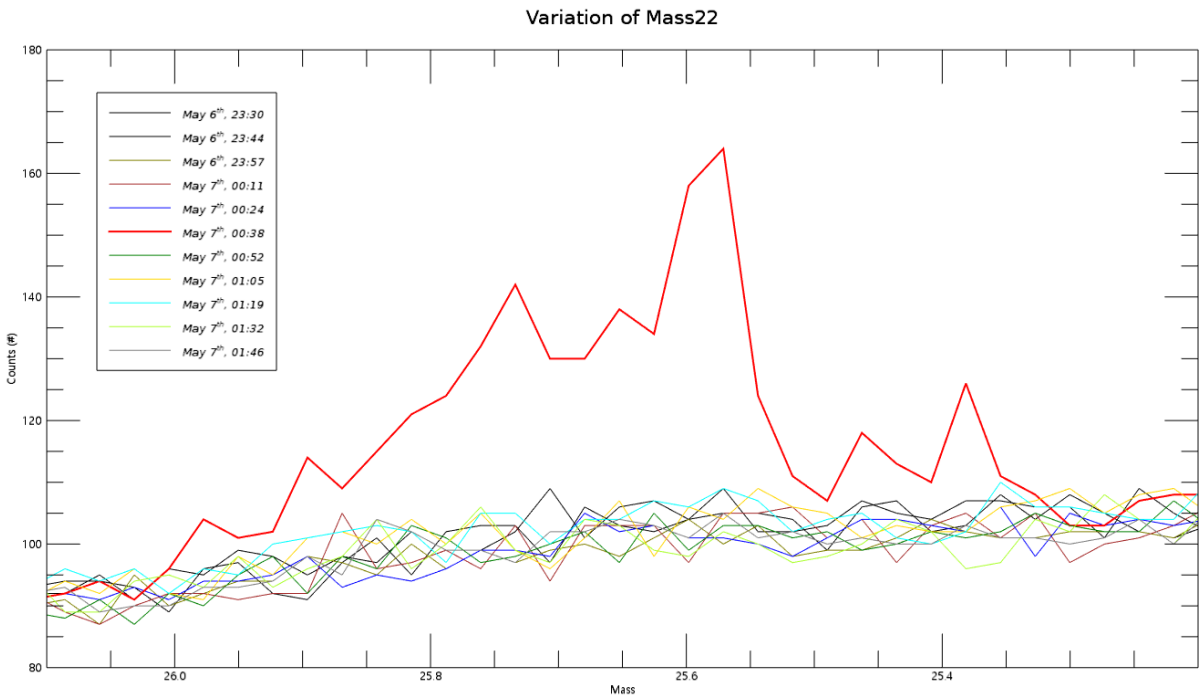

Figure S15.Variation of Mass 22 May 6 - May 7 showing a quick increase followed by decrease.

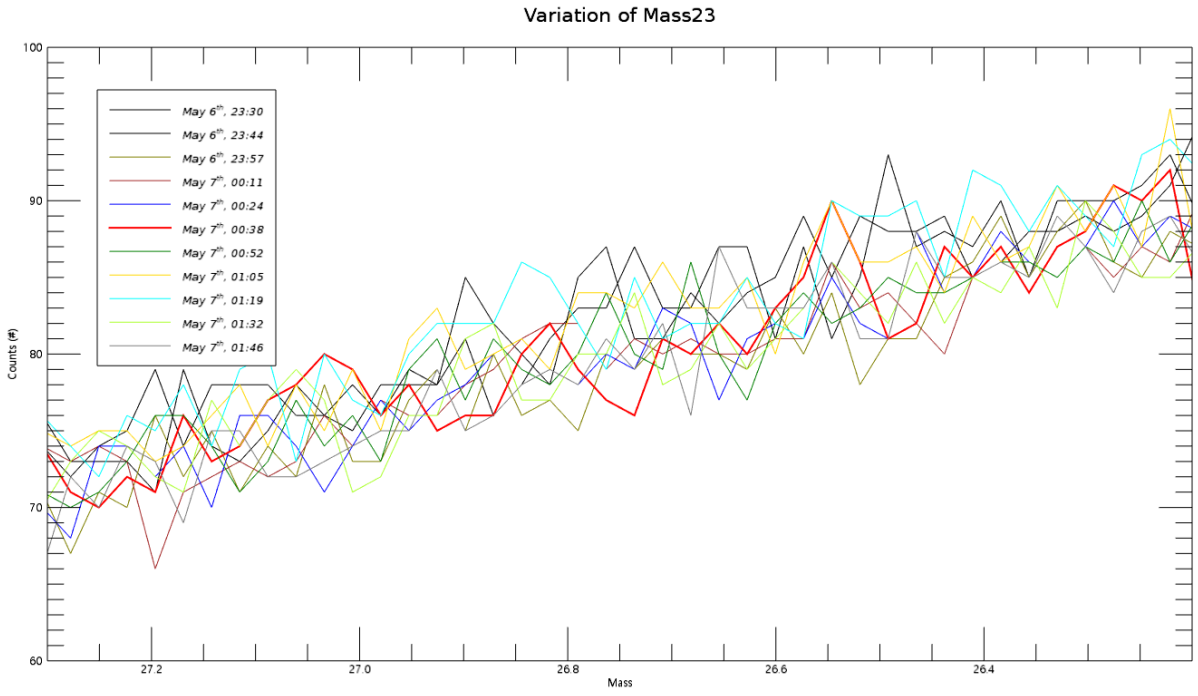

Figure S16.Variation of Mass 23 May 6 - May 7 (noise).

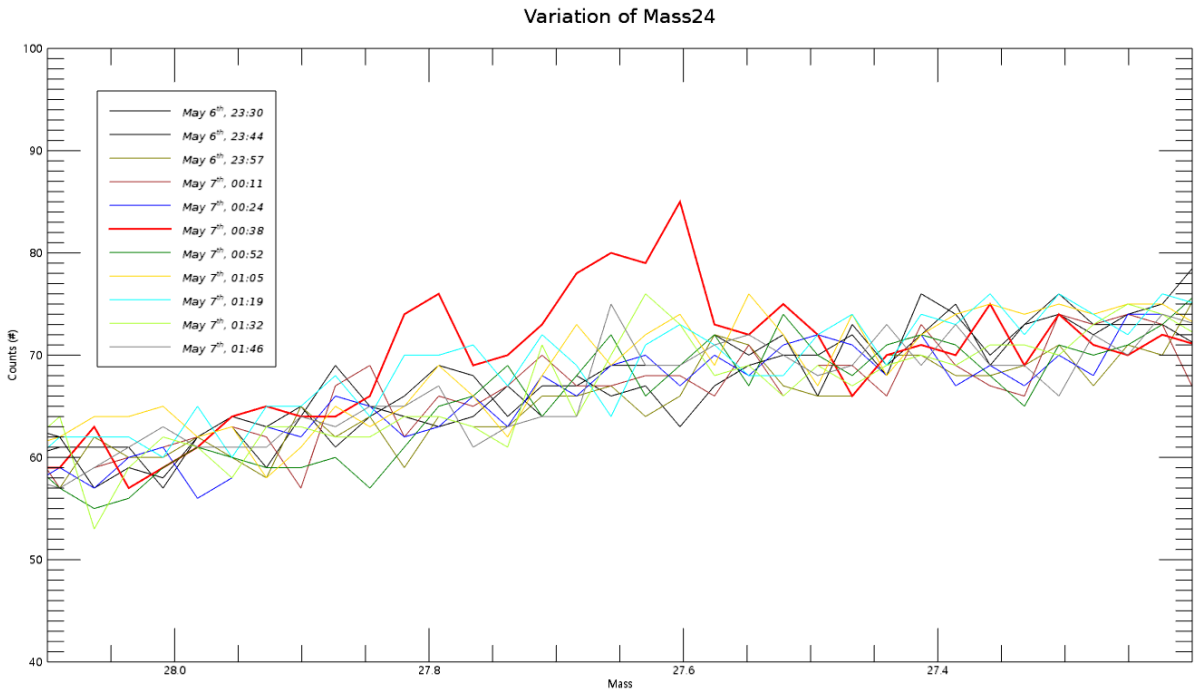

Figure S17.Variation of Mass 24 May 6 - May 7 showing a small increase.

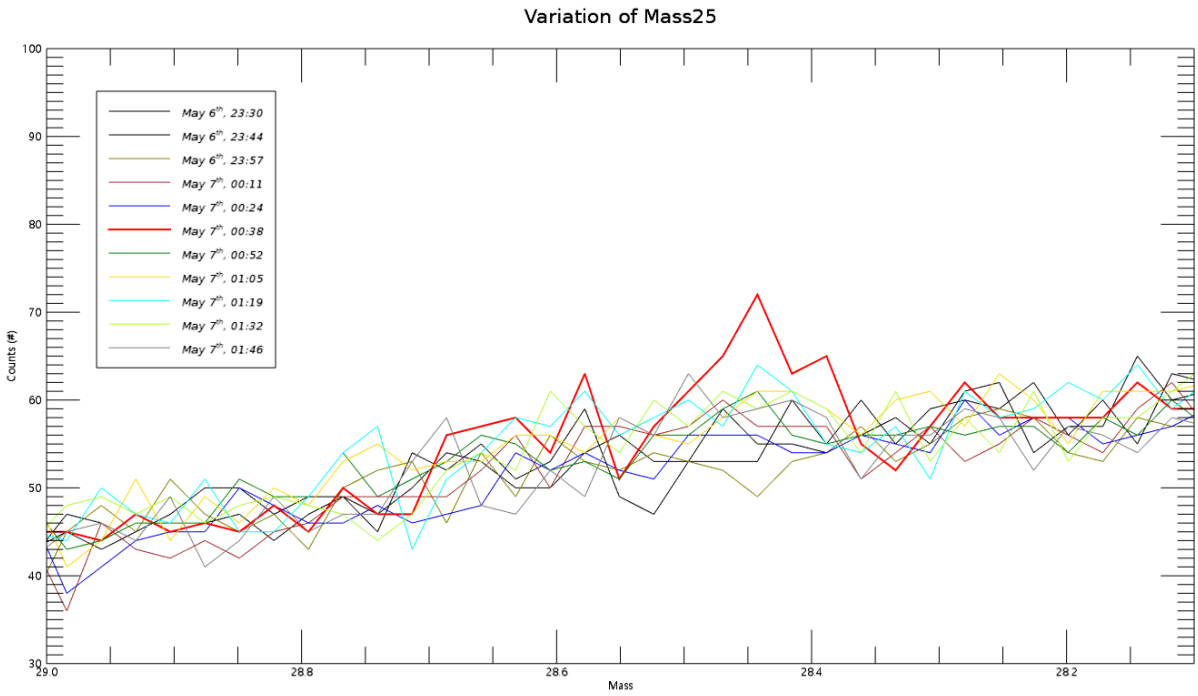

Figure S18.Variation of Mass 25 May 6 - May 7 showing a small increase.

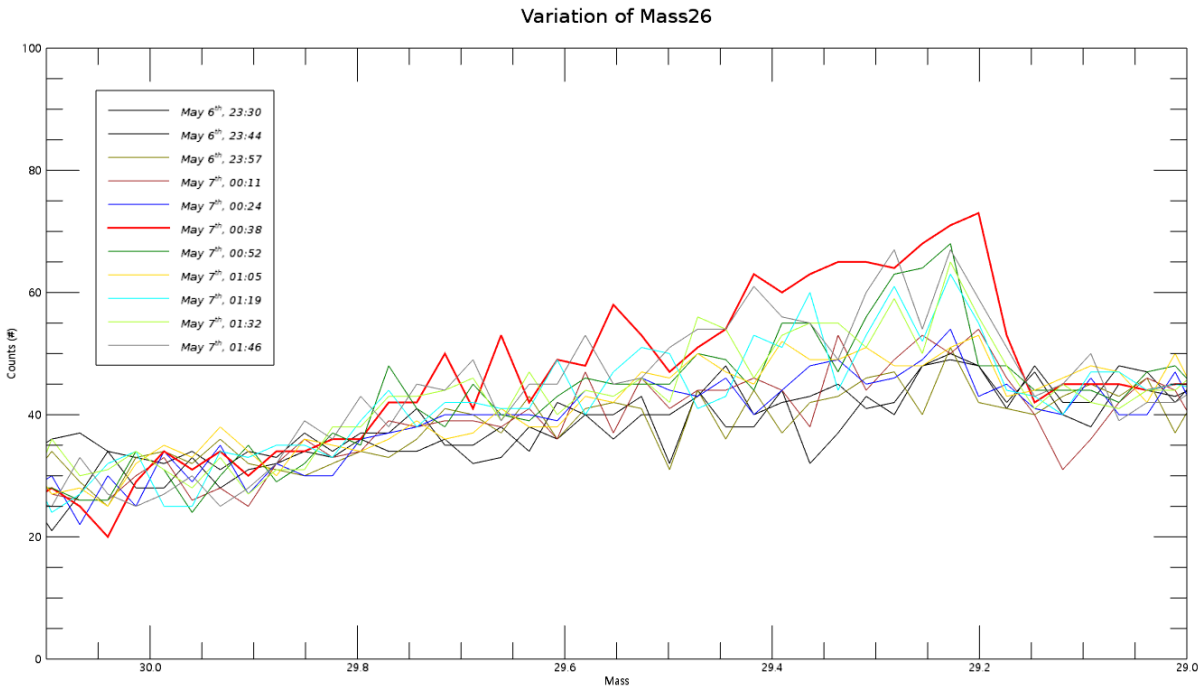

Figure S19.Variation of Mass 26 May 6 - May 7 showing probably noise.

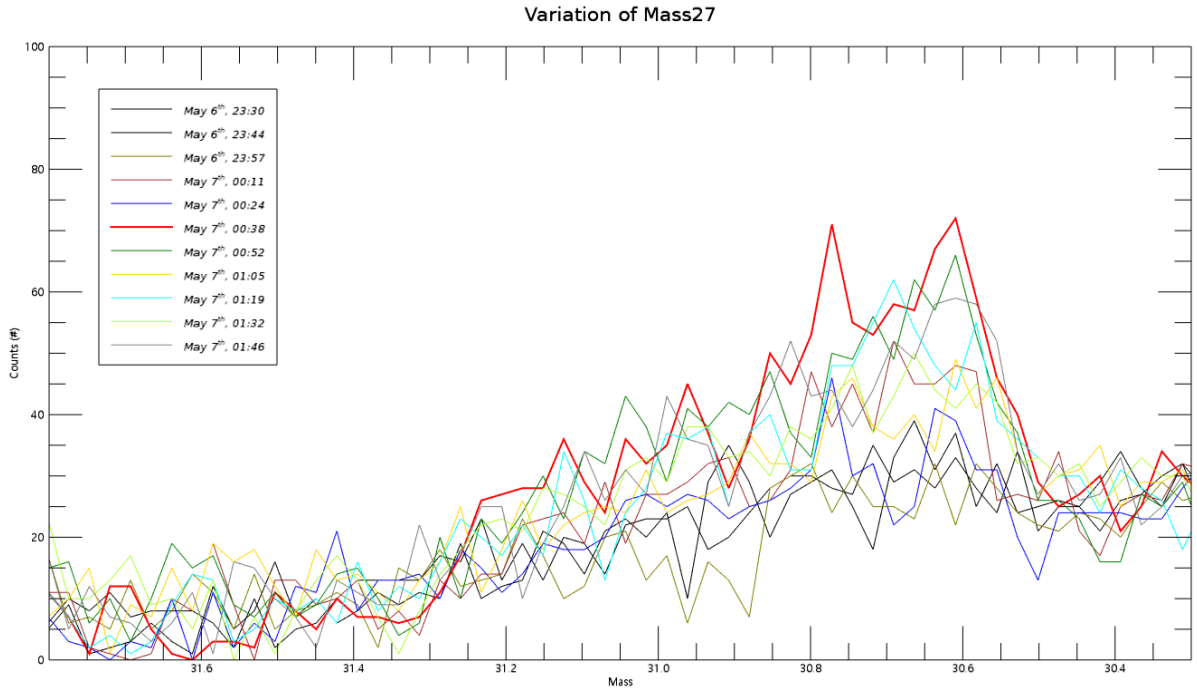

Figure S20.Variation of Mass 27 May 6 - May 7 showing small increase.

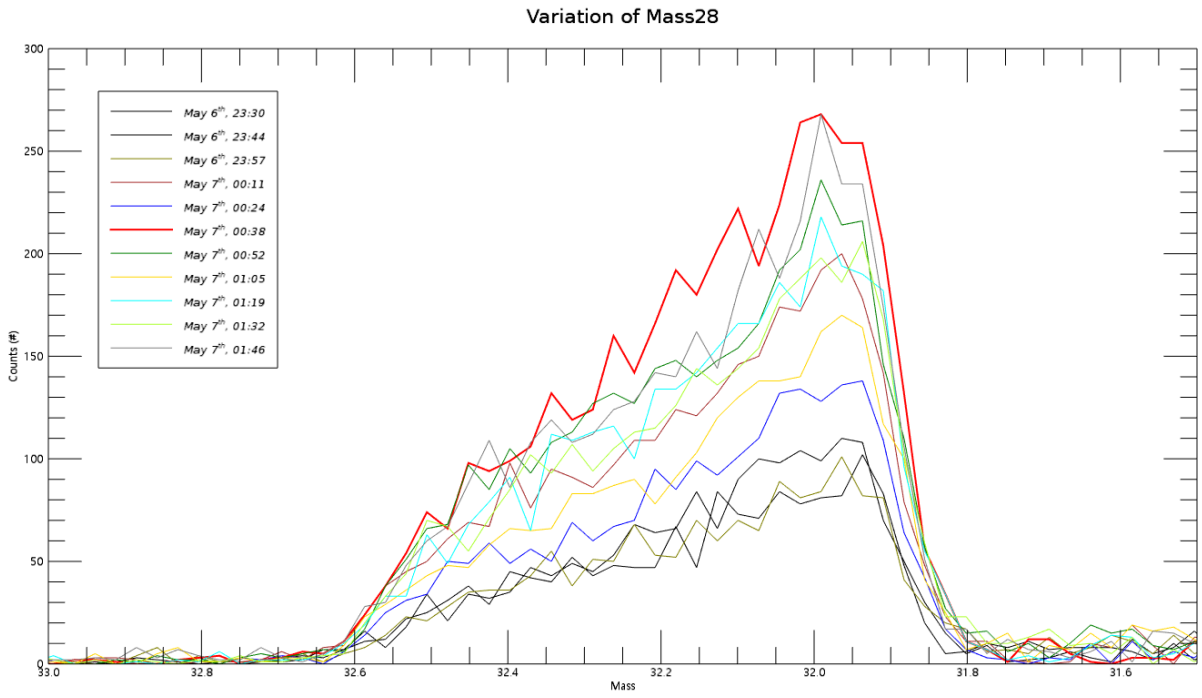

Figure S21.Variation of Mass 28 May 6 - May 7 showing gradual increase.

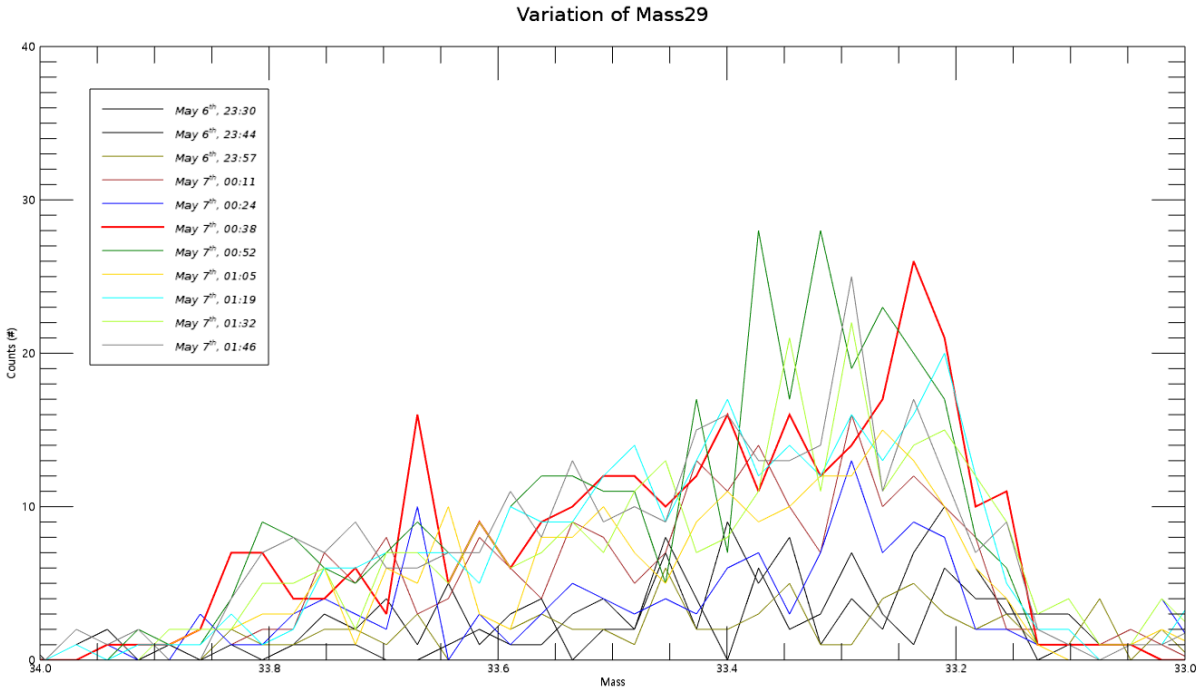

Figure S22.Variation of Mass 29 May 6 - May 7 showing gradual increase.

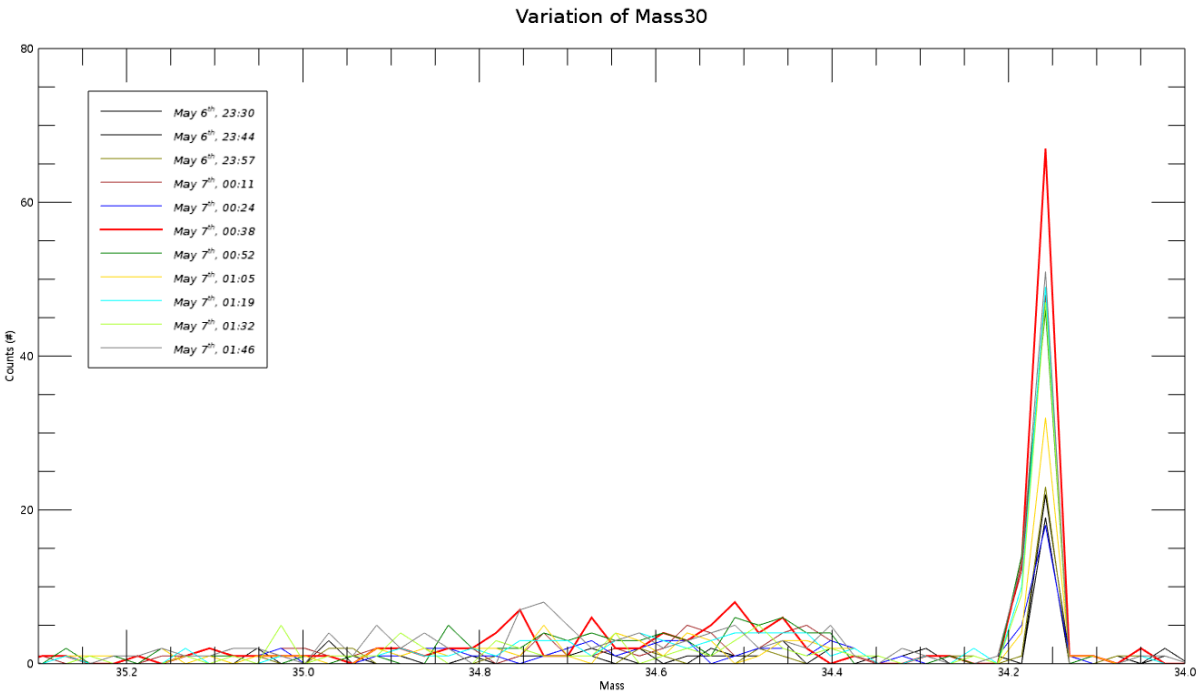

Figure S23.Variation of Mass 30 May 6 - May 7 showing the sharp peak at right side is noise.

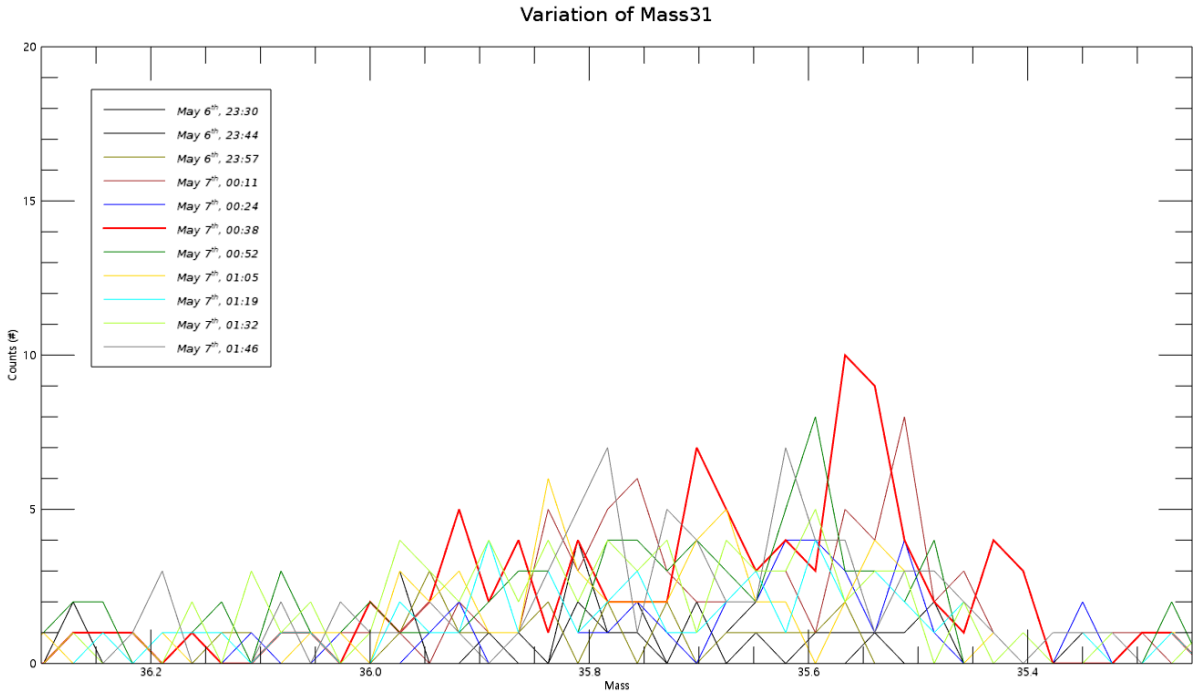

Figure S24.Variation of Mass 31 May 6 - May 7 showing noise.

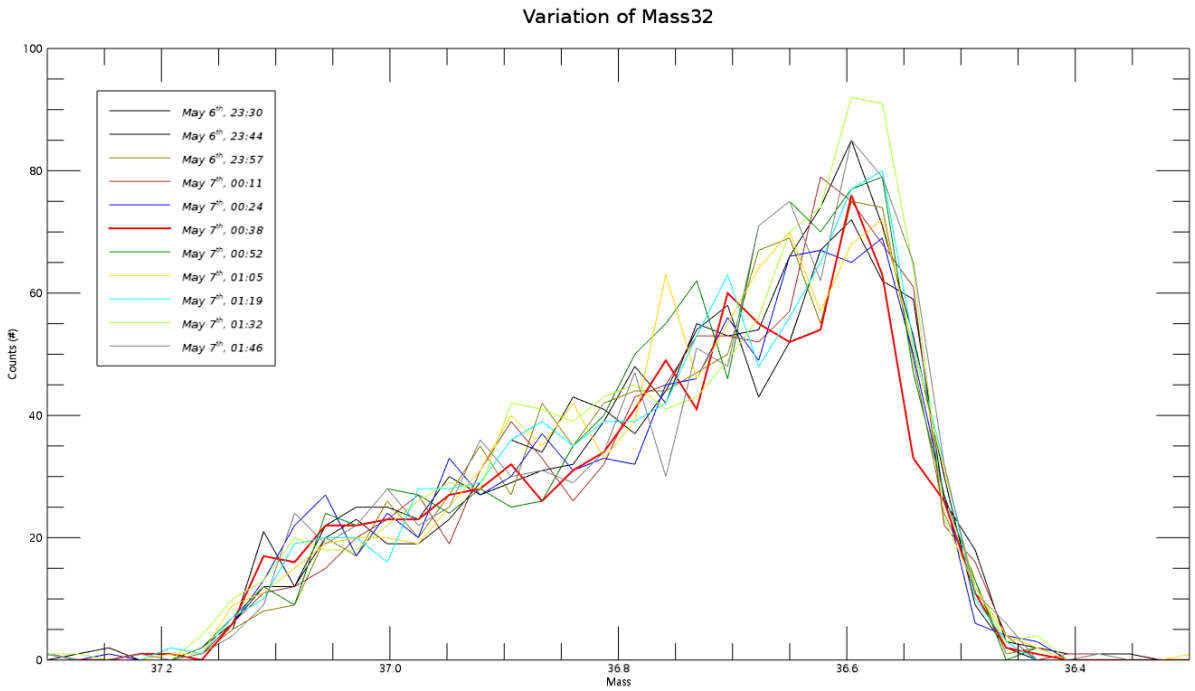

Figure S25.Variation of Mass 32 May 6 - May 7 showing no increase.

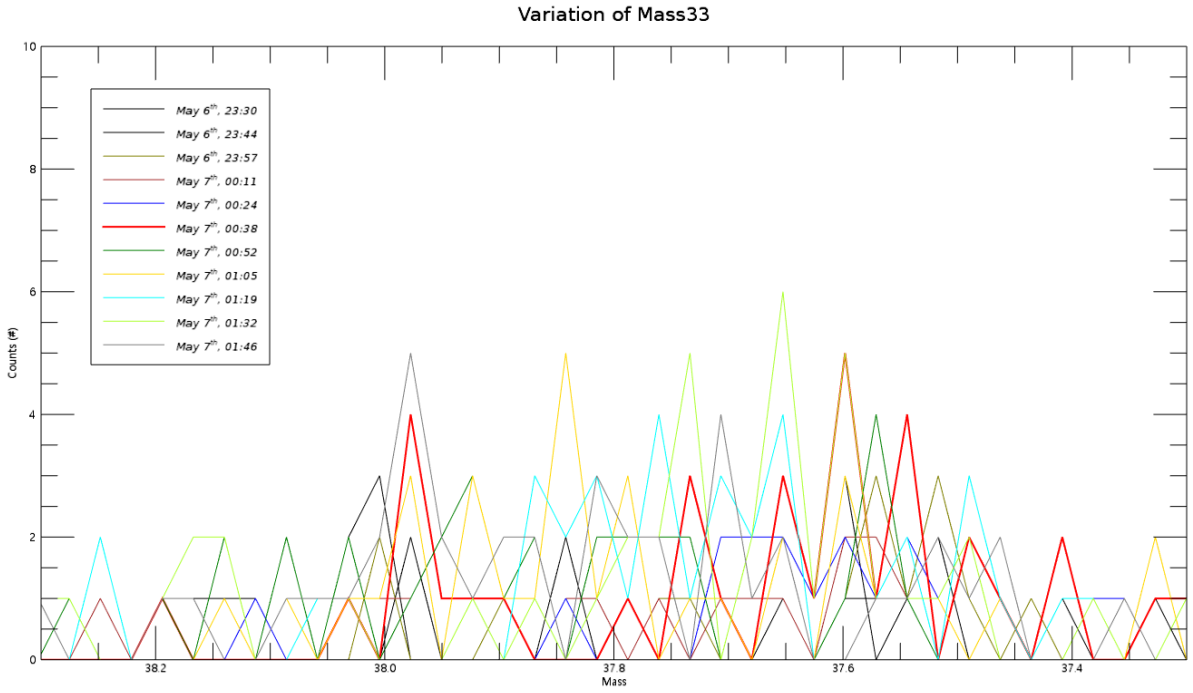

Figure S26.Variation of Mass 33 May 6 - May 7 showing noise.

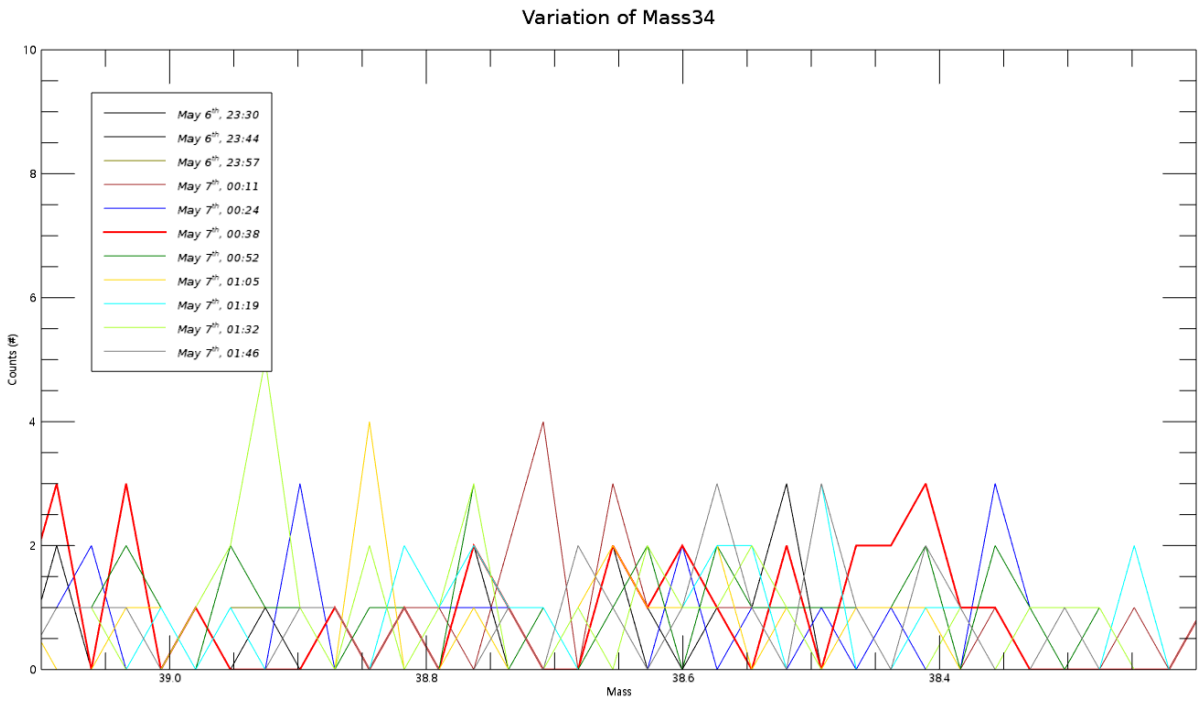

Figure S27.Variation of Mass 34 May 6 - May 7 showing noise.

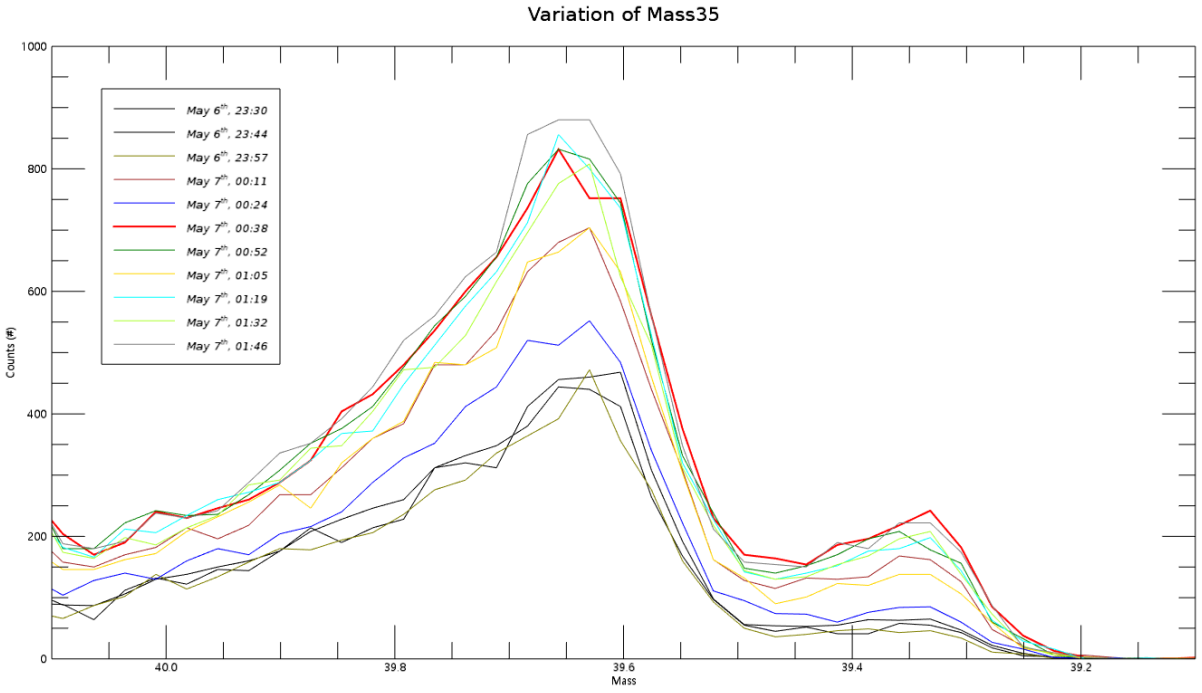

Figure S28.Variation of Mass 35 May 6 - May 7 showing gradual increase.

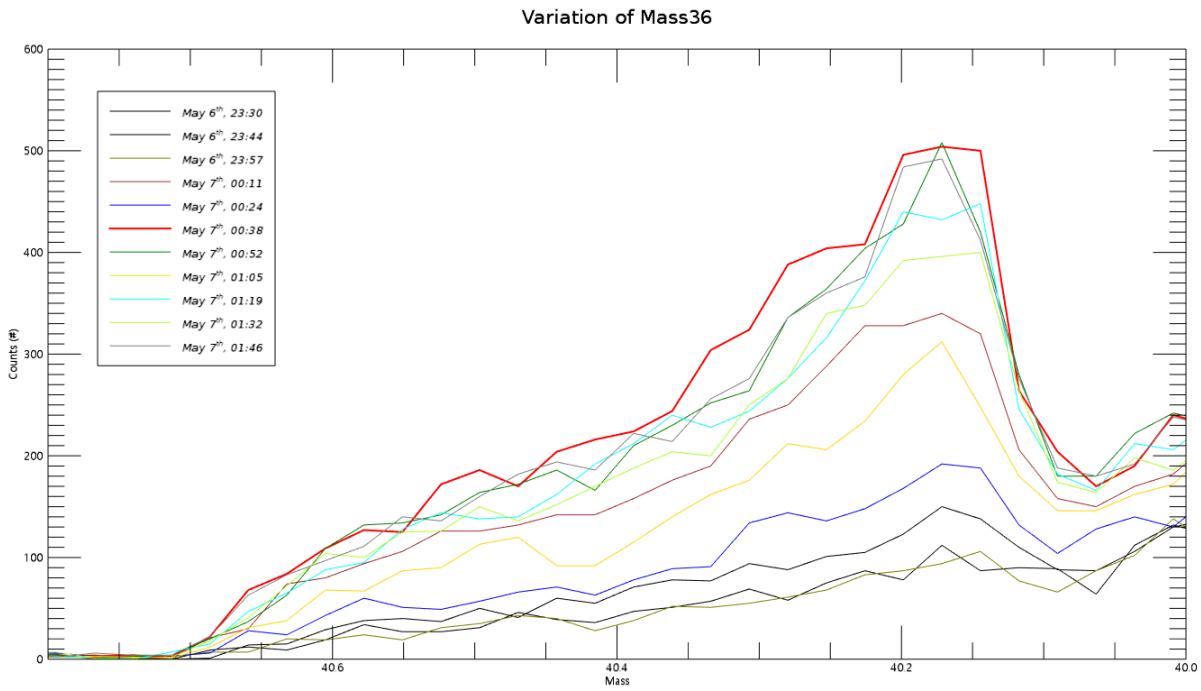

Figure S29.Variation of Mass 36 May 6 - May 7 showing gradual increase.

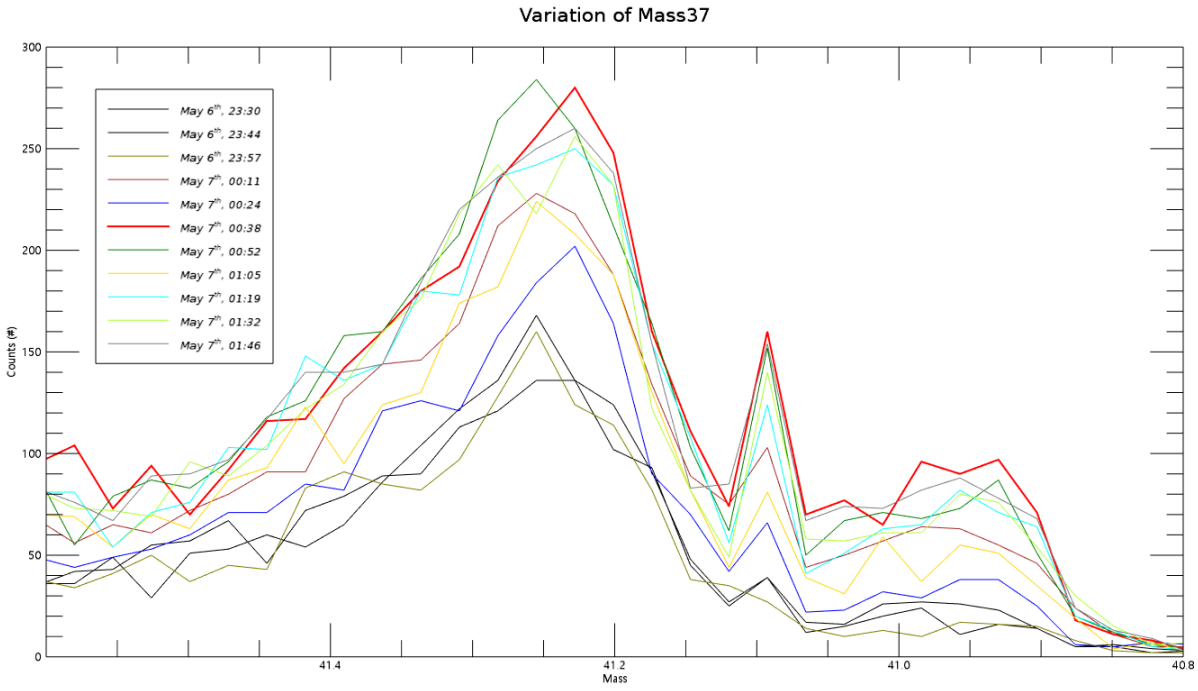

Figure S30.Variation of Mass 37 May 6 - May 7 showing gradual increase.

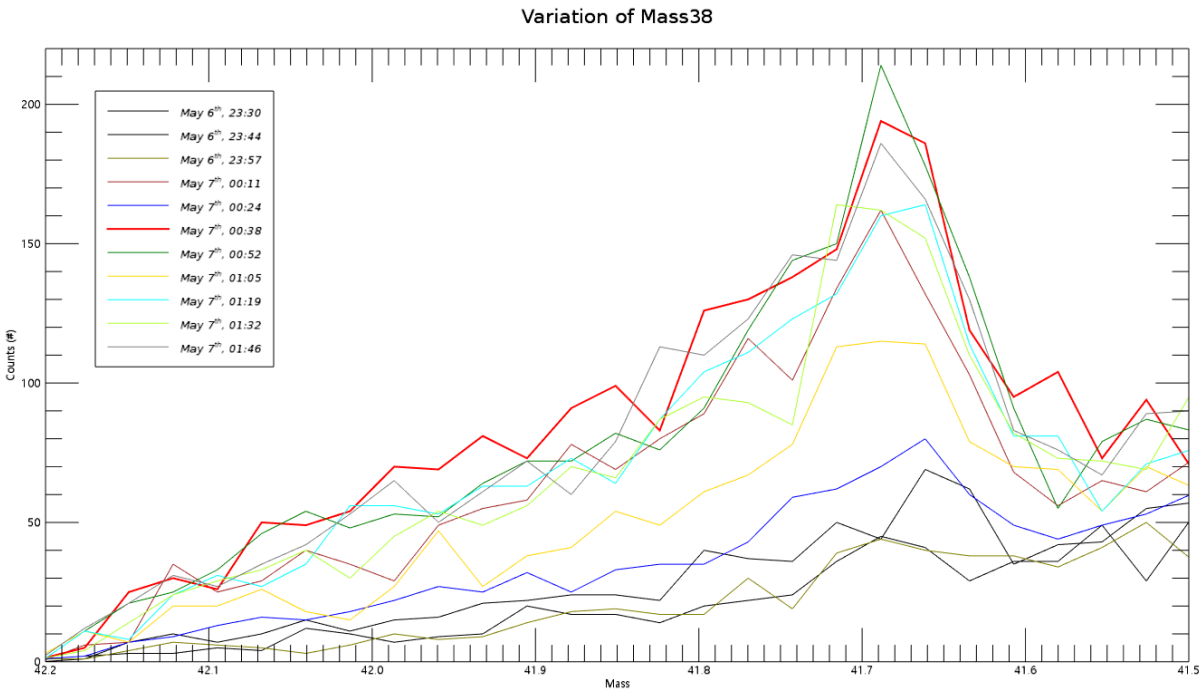

Figure S31.Variation of Mass 38 May 6 - May 7 showing gradual increase.

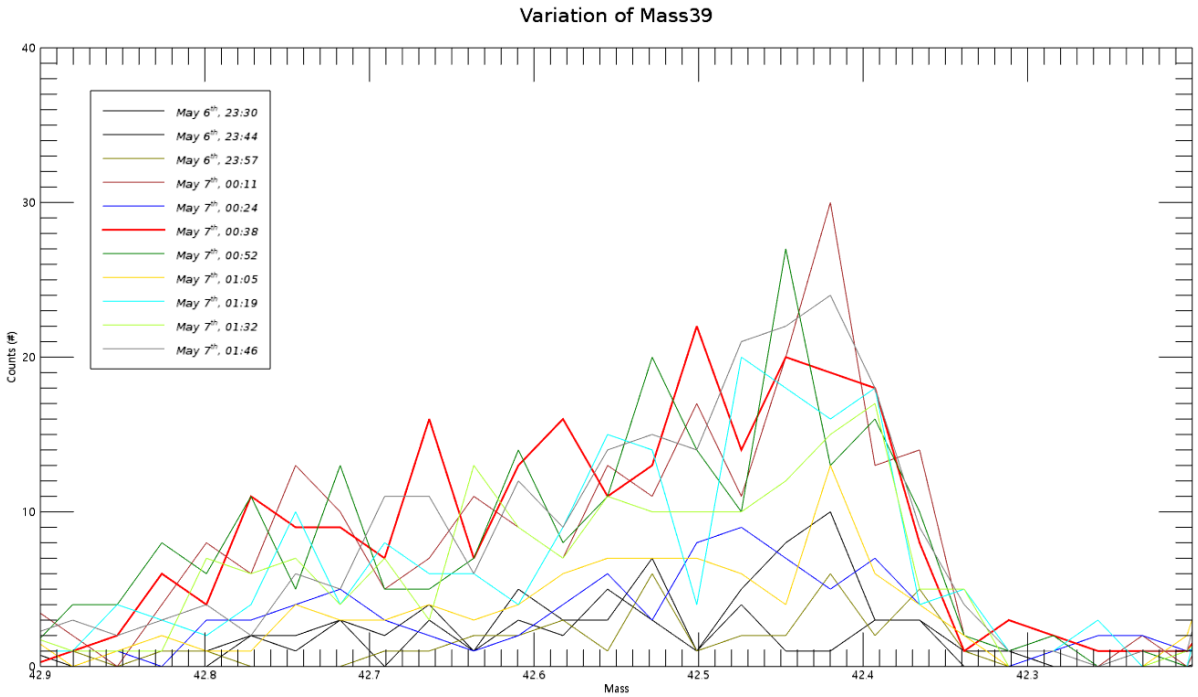

Figure S32.Variation of Mass 39 May 6 - May 7 showing gradual increase.

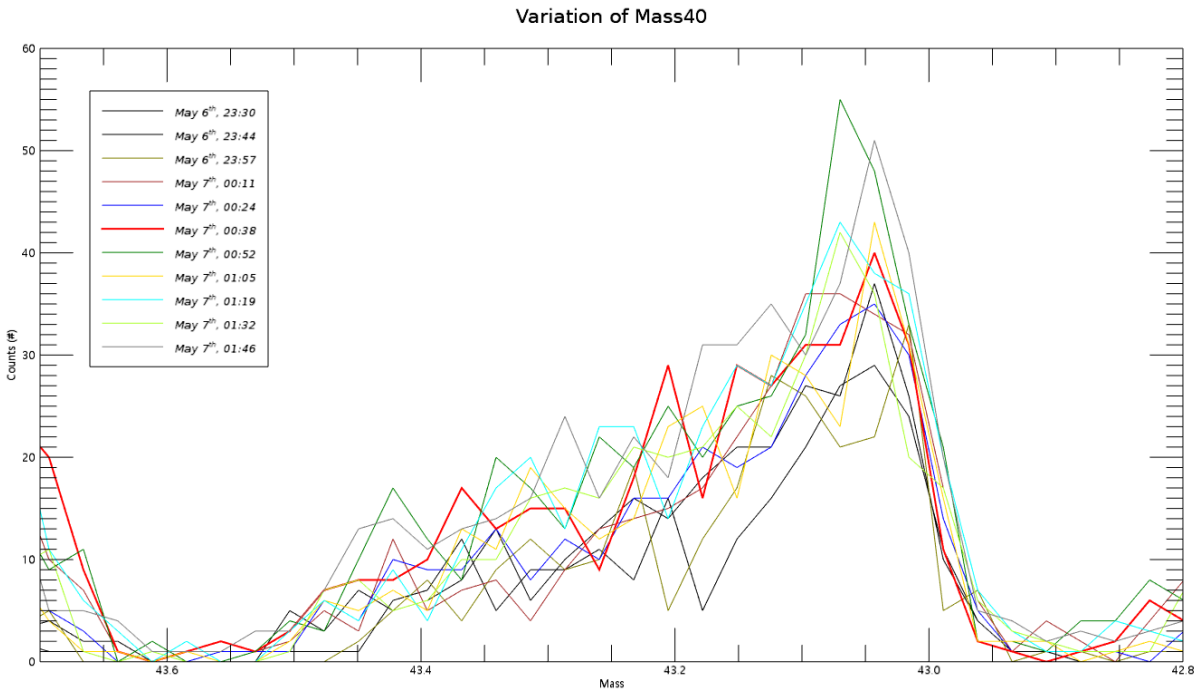

Figure S33.Variation of Mass 40 May 6 - May 7.

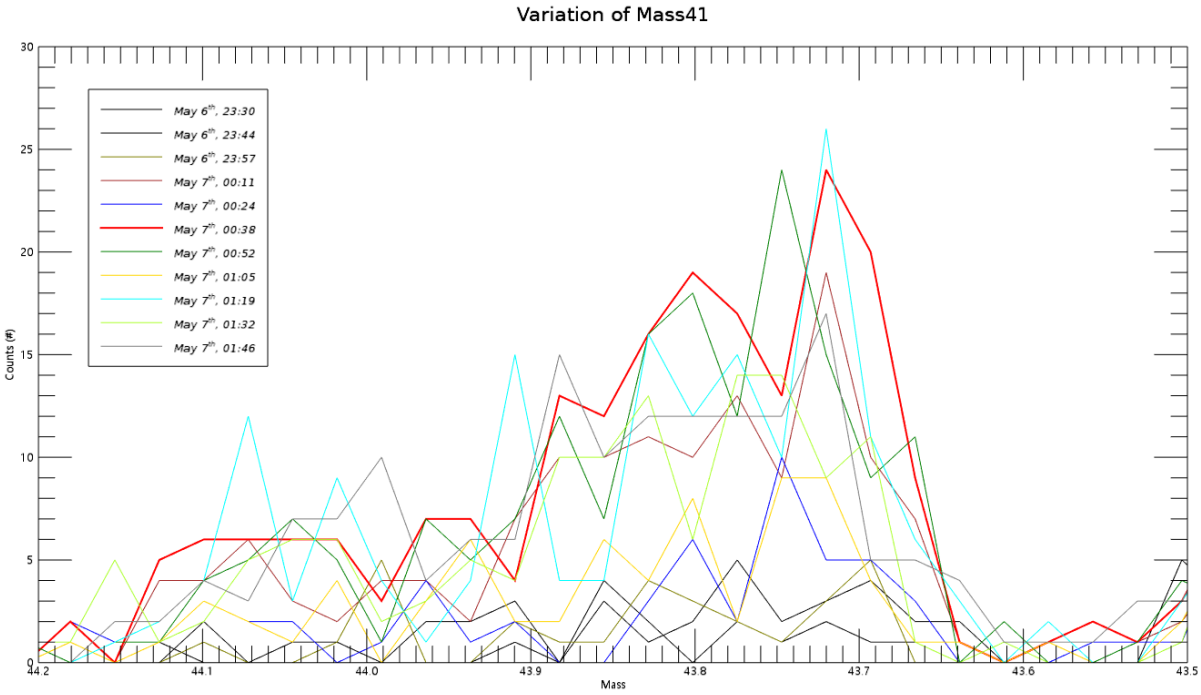

Figure S34.Variation of Mass 41 May 6 - May 7.

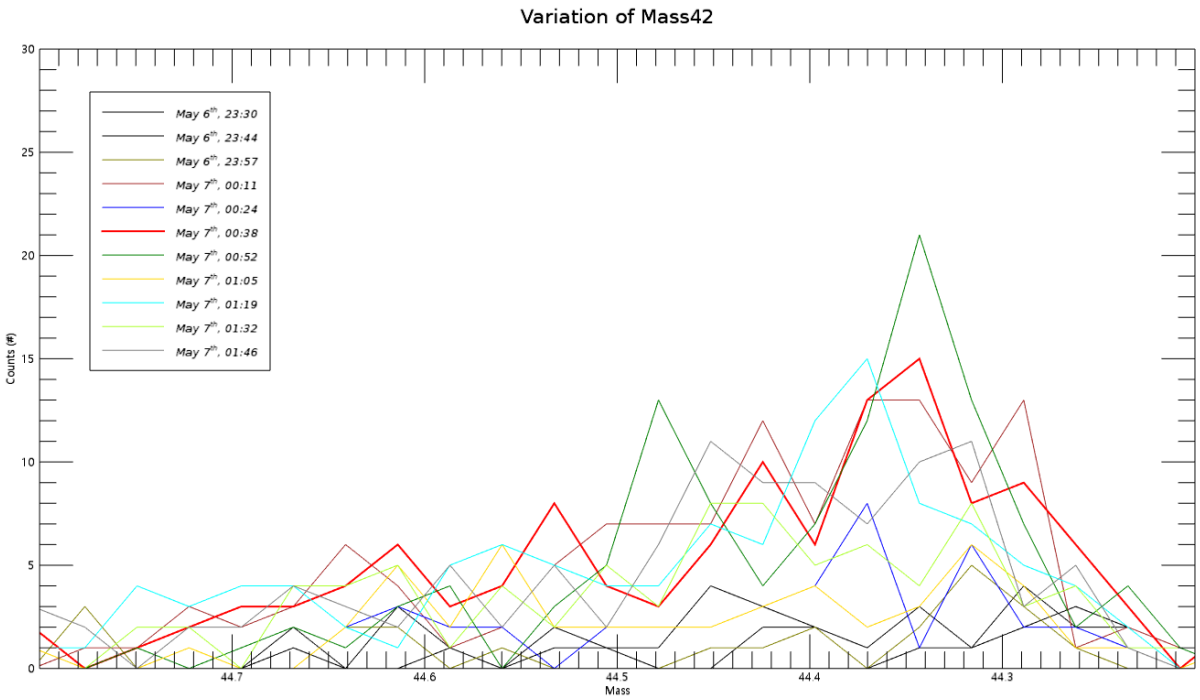

Figure S35.Variation of Mass 42 May 6 - May 7.

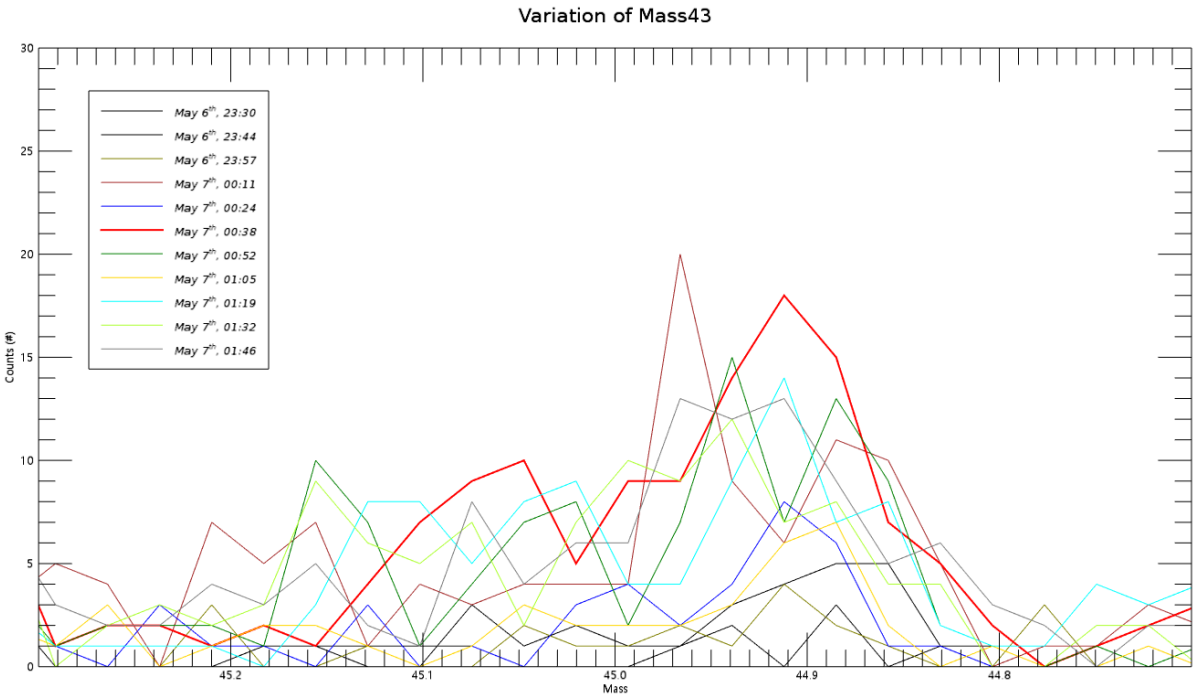

Figure S36.Variation of Mass 43 May 6 - May 7.

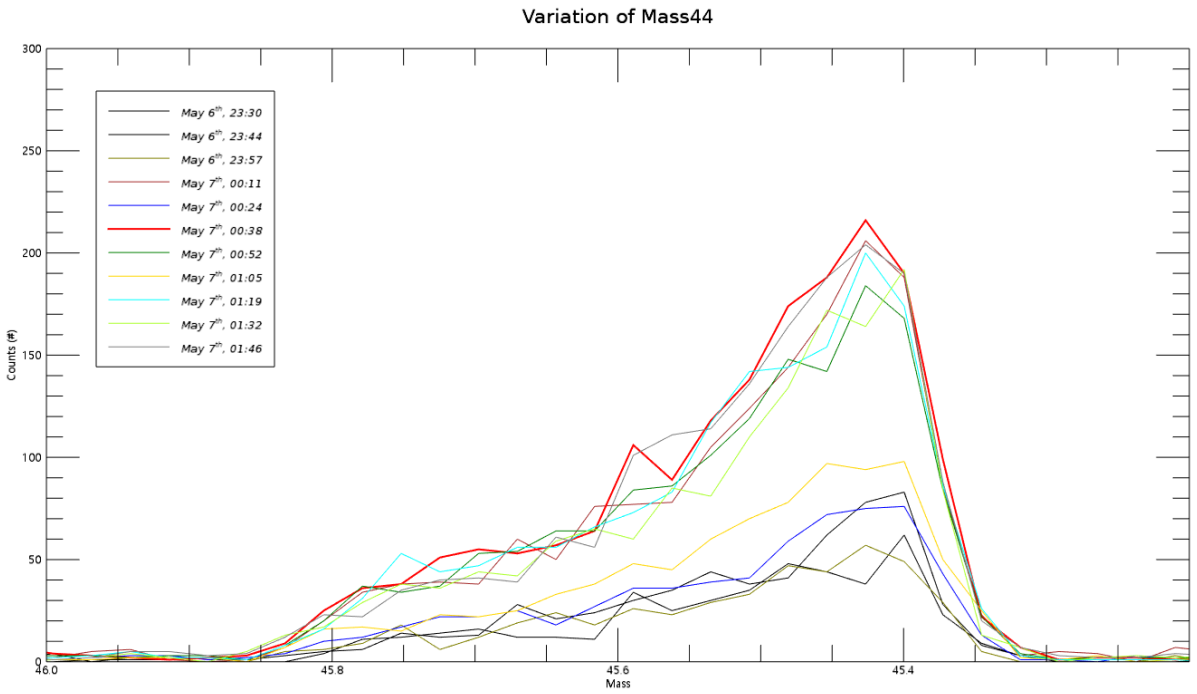

Figure S37.Variation of Mass 44 May 6 - May 7.

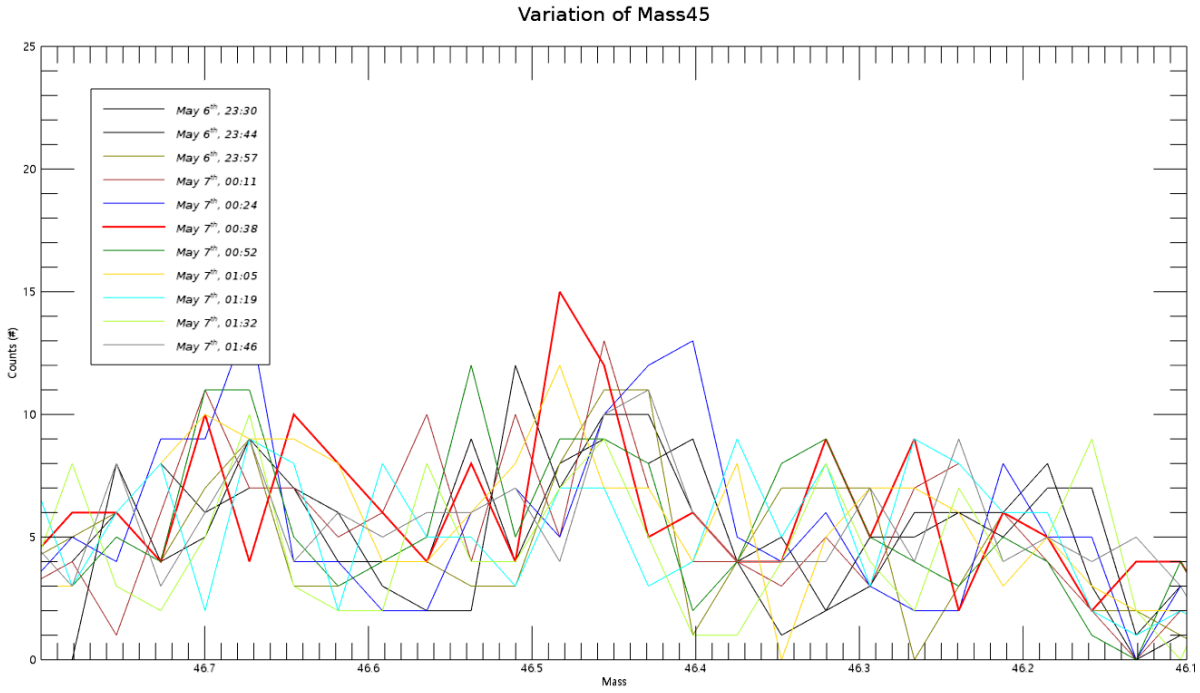

Figure S38.Variation of Mass 45 May 6 - May 7 showing noise.

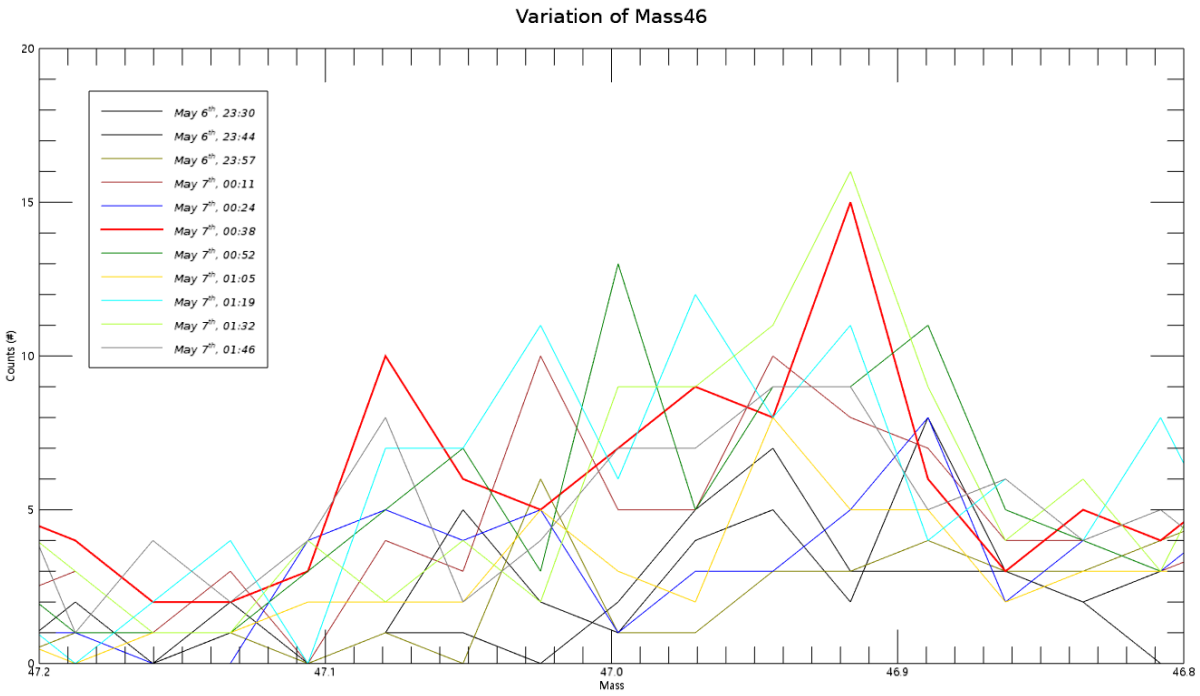

Figure S39.Variation of Mass 46 May 6 - May 7 probably showing noise.

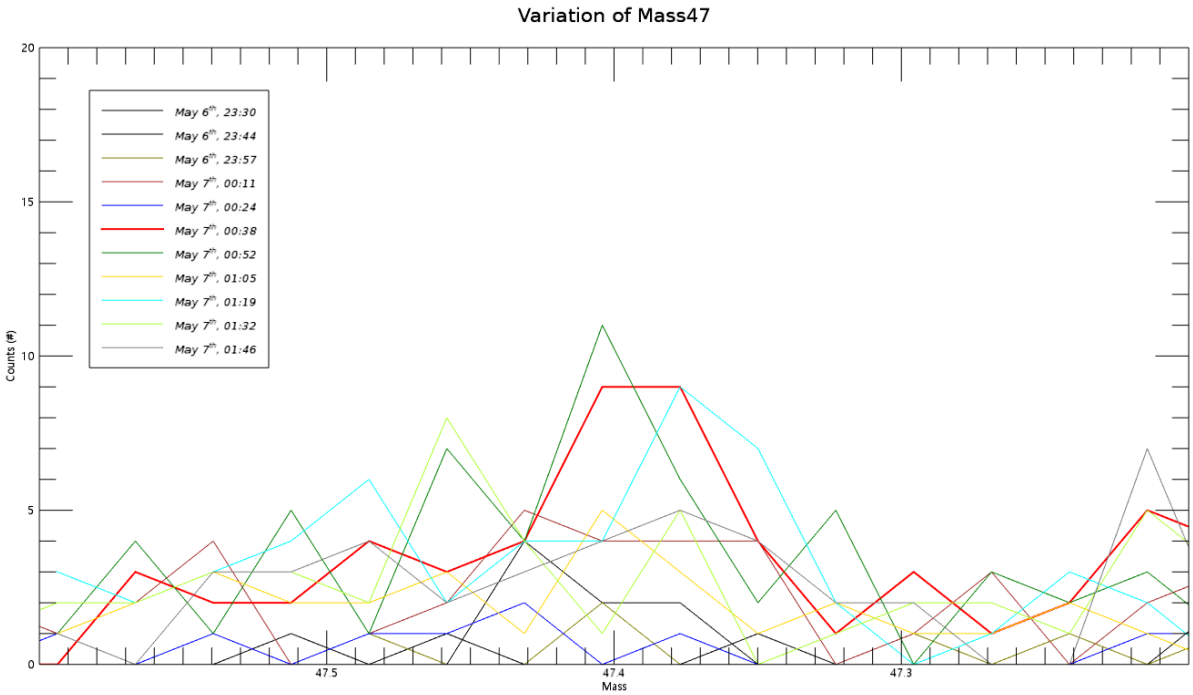

Figure S40.Variation of Mass 47 May 6 - May 7 probably showing noise.

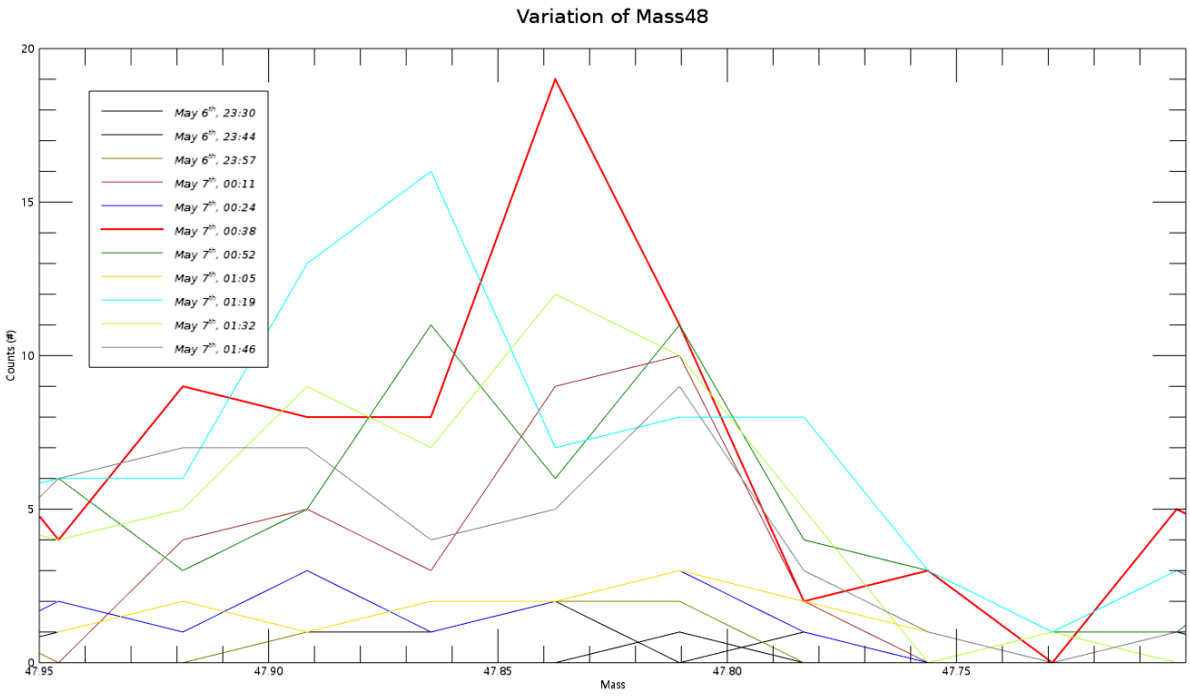

Figure S41.Variation of Mass 48 May 6 - May 7 probably showing noise.

S.4 Simulation (3) of neon density at TL using the OMNI SW flux

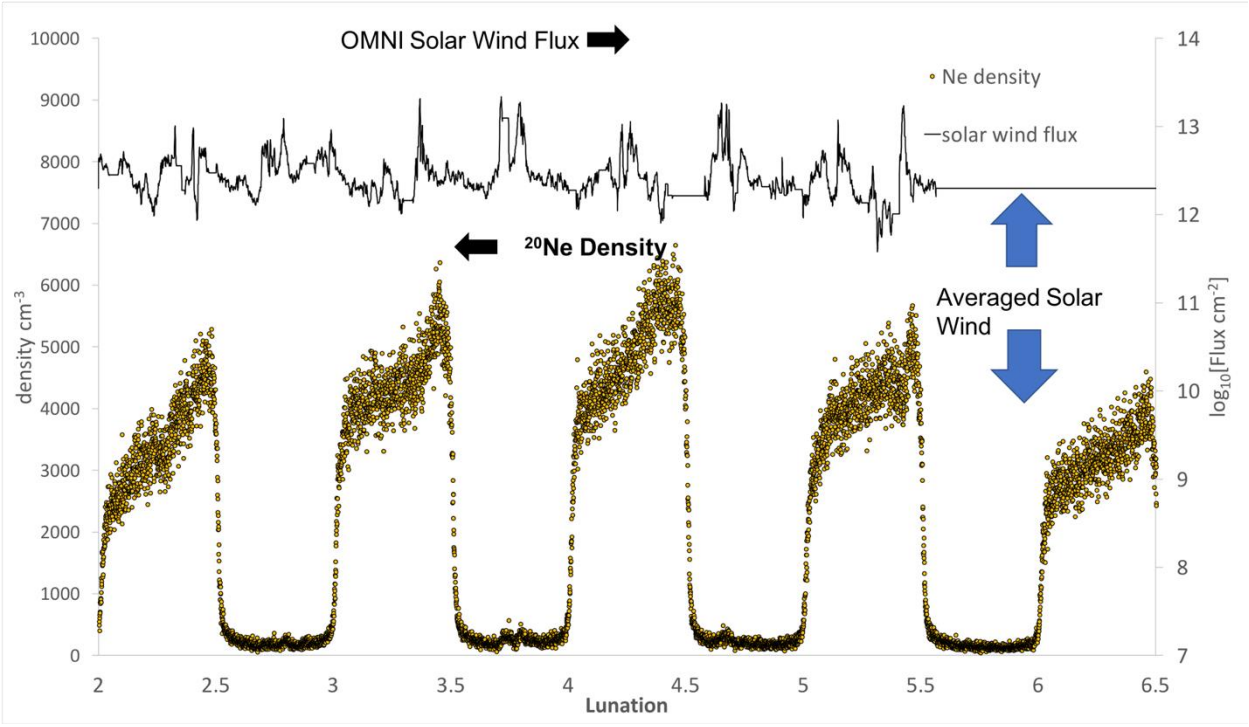

528

Figure S42: Simulation (3) of neon density at TL using the SW flux from omniweb.gsfc.nasa.gov, and the artificial lifetime of 4.5 days. Omniweb has paths to Magnetic field, Plasma, Energetic particle data relevant to heliospheric studies and resident at Goddard's Space Physics Data Facility (Smith and Barnes, 2018; King and Papatashvili, 2018).

529 We also modeled the effect of solar wind variability during the experiment, because Ne is inert

530 and typically considered to be in dynamic equilibrium with the solar wind ion flux. However, we

531 found the solar wind variability could not account for the decrease in ^{20}Ne densities measured by

532 LACE during the 4th and 5th lunations, nor the spurious increases measured densities measured

533 near the terminator during lunation 5. While the increase in densities near the terminators is

534 likely an instrumental artifact, the peculiar trend of the decrease in density over the lunar night

during lunations 2 and 3 appear to be real. Therefore, our analyses and model results support the need for future experiments.